Open access • Posted Content • DOI:10.1101/2021.02.07.430164

A viral protein utilizes the NDP52/CALCOCO2 selective autophagy receptor to disassemble processing bodies — Source link

Carolyn-Ann Robinson, Carolyn-Ann Robinson, Gillian K. Singh, Elizabeth L. Castle ...+3 more authors

Institutions: University of Calgary, Dalhousie University

Published on: 08 Feb 2021 - bioRxiv (Cold Spring Harbor Laboratory)

Topics: ATG5, Autophagy and Gene silencing

The NDP52/CALCOCO2 selective autophagy receptor controls processing body disassembly

inflammatory cytokine transcripts / Kaposi's sarcoma-associated herpesvirus / NDP52 / processing bodies / selective autophagy

Carolyn-Ann Robinson[1,2,3,4], Gillian K. Singh[1,4], Elizabeth L. Castle[1], Bre Q. Boudreau[1], Jennifer A. Corcoran[1,2,3,5]

[1]Department of Microbiology & Immunology, Dalhousie University, Halifax, NS, Canada

[2]Microbiology, Immunology & Infectious Diseases Department, University of Calgary, Calgary, AB, Canada.

[3]Charbonneau Cancer Research Institute, University of Calgary, Calgary, AB, Canada.

[4]Equal Contribution

[5]Corresponding Author

Abstract

Processing bodies (PBs) are cytoplasmic ribonucleoprotein granules that control inflammation by silencing or degrading labile messenger RNAs (mRNAs) that encode inflammatory molecules. PBs often disassemble in response to virus infection, which correlates with increased synthesis of inflammatory proteins. We previously showed that the Kaposi's sarcoma-associated herpesvirus (KSHV) KapB protein causes PB disassembly. Here, we reveal that KapB-mediated PB disassembly depends on the canonical autophagy genes *Atg5* and *Atg14* or the selective autophagy receptor *NDP52/CALCOCO2*. Moreover, KapB expression increased inflammatory transcripts levels and this effect was also dependent on canonical autophagy and NDP52. Stimulating autophagy with the mTOR inhibitor Torin-1 also increased cytokine mRNA and required ATG5 and NDP52 to mediate PB disassembly. These studies reveal a new role for NDP52 in regulating inflammatory responses by promoting PB turnover and the concomitant synthesis of inflammatory molecules.

Introduction

Under basal conditions, autophagic activity ensures the continuous recycling of cellular resources and the clearance of damaged macromolecular complexes and organelles, maintaining cellular homeostasis and acting as an intracellular quality control system (Green *et al*, 2011; Klionsky *et al*, 2012; Morishita & Mizushima, 2019; Levine *et al*, 2008). Various changes to the cellular microenvironment, including nutrient scarcity, hypoxia, and endoplasmic reticulum (ER) stress can drive autophagy and degradation of damaged organelles (e.g mitochondria, peroxisomes), protein complexes (e.g. focal adhesion complexes), or other targets in a selective manner (Maiuri & Kroemer, 2015; Mizushima *et al*, 2010; Balgi *et al*, 2009; Kenific *et al*, 2016; Sargsyan *et al*, 2015; Tripathi *et al*, 2016; Dunn *et al*, 2005; Yao & Klionsky, 2016). In selective autophagy, target cargo is selected for degradation either directly, by binding to lipidated microtubule associated protein 1 light chain 3 (LC3) protein (LC3-II), or indirectly via molecular bridges termed selective autophagy receptors (SARs). Some of the best characterized SARs include p62/SQSTM1, valosin containing protein (VCP), optineurin (OPTN), neighbor of BRCA1 gene 1 (NBR1), and nuclear dot protein 52 (NDP52/calcium binding and coiled-coil domain protein, CALCOCO2) (Zaffagnini & Martens, 2016). OPTN, p62, NDP52, and NBR1 are members of the sequestosome-like family and contain several conserved motifs including a LC3-interacting region (LIR) and a ubiquitin-binding domain (UBD) (Ichimura *et al*, 2008; Noda *et al*, 2010; Birgisdottir *et al*, 2013; Noda *et al*, 2008). The selection of cargo for degradation can occur in a ubiquitin-dependent or -independent manner, although ubiquitin modification is believed to enhance cargo recruitment to autophagosomes (Rogov *et al*, 2014). SARs play important homeostatic roles in maintaining, and at times magnifying, the turnover of organelles and aggregates which facilitates cell survival in response to environmental changes

(Maiuri & Kroemer, 2015; Mizushima *et al*, 2010; Balgi *et al*, 2009; Kenific *et al*, 2016; Sargsyan *et al*, 2015; Tripathi *et al*, 2016; Dunn *et al*, 2005; Yao & Klionsky, 2016).

SARs also play important roles in fine-tuning innate immune responses by targeting key signaling platforms for degradation (Chen *et al*, 2016; Du *et al*, 2018; Jin *et al*, 2017; Prabakaran *et al*, 2018; Yang *et al*, 2017; He *et al*, 2019). For example, NDP52 is required for the autophagic degradation of interferon regulatory factor 3 (IRF3) and mitochondrial antiviral signaling protein (MAVS), which supports the resolution phase of type I interferon signaling (Wu *et al*, 2020) (Seth *et al*, 2005; Jin *et al*, 2017). Both pro and antiviral roles have been attributed to SARs (Sumpter & Levine, 2011; Ahmad *et al*, 2018) and viruses can both enhance or limit SAR function accordingly, promoting their replication (Mohamud *et al*, 2019). Kaposi's sarcoma-associated herpesvirus (KSHV) is the infectious cause of two B-cell malignancies and the endothelial cell cancer, Kaposi's sarcoma (KS), which is typified by aberrant angiogenesis, tortuous leaky blood vessels, and inflammation (Cesarman *et al*, 1995; Chang *et al*, 1994; Soulier *et al*, 1995). Infection with KSHV has two forms, a latent and a lytic phase and it is the latent phase that predominates in KS tumours (Decker *et al*, 1996; Staskus *et al*, 1997; Broussard & Damania, 2020). Like many viruses, KSHV manipulates the autophagic machinery. During latency, the viral FLICE inhibitory protein (v-FLIP) binds Atg3 to suppress the LC3 lipidation process during autophagosome biogenesis (Lee *et al*, 2009). KSHV also expresses a viral cyclin D homolog (v-cyclin), that triggers DNA damage that that leads to autophagy and cellular senescence (Leidal *et al*, 2012), facilitating the production and non-conventional secretion of pro-inflammatory cytokines such as IL-1β, IL-6 and IL-8 (Young *et al*, 2009). Together, KSHV manipulation of autophagic flux prevents xenophagy, limits interferon

responses and enhances inflammatory cytokine production. Precisely how KSHV fine tunes autophagy during latency to balance proviral and antiviral activities and promote chronic viral infection is not clear.

Processing bodies (PBs) are ubiquitous, cytoplasmic, ribonucleoprotein (RNP) granules that regulate expression of many cytokine RNA transcripts, making them important sites of inflammatory control. PBs contain enzymes involved in mRNA turnover, including those that mediate decapping (Dcp2; co-factors Dcp1a and Edc4/Hedls), 5'-3' exonucleolytic degradation (5'-3' exonuclease Xrn1 and RNA helicase Rck/DDX6) and some components of the RNA-induced silencing complex (Cougot *et al*, 2012; Hubstenberger *et al*, 2017; Corbet & Parker, 2019; Youn *et al*, 2018; Riggs *et al*, 2020; Mohamud *et al*, 2019; Luo *et al*, 2018). mRNAs are routed to PBs for decay and/or repression by RNA-binding proteins (RBPs) through recognition of common sequence elements (Hubstenberger *et al*, 2017). AU-rich elements (AREs) are destablilizing RNA regulatory elements found in the 3' untranslated regions of ~8% of cellular transcripts that are responsible for targeting RNAs to PBs (Barreau *et al*, 2005; Bakheet *et al*, 2018; García-Mauriño *et al*, 2017). When bound by destabilizing RBPs, ARE-containing RNAs are directed to PBs and suppressed (Maitra *et al*, 2008; Lai *et al*, 1999; Lai & Blackshear, 2001). Our group and others showed that microscopically visible PBs correlate with the constitutive turnover or translational suppression of ARE-mRNAs; when PBs are dispersed, this suppression is reversed (Corcoran *et al*, 2012, 2015; Franks & Lykke-Andersen, 2007; Blanco *et al*, 2014; Vindry *et al*, 2017). Because ARE-mRNAs code for potent regulatory molecules such as inflammatory cytokines, PBs are important post-transcriptional regulator that fine tune the production of inflammatory cytokines whose transcripts contain AREs, including IL-6, IL-8, IL-

1β, and TNF (Ensoli *et al*, 2010; Ensoli & Stürzl, 1998; Lane *et al*, 2002; Miles *et al*, 1990; Riva *et al*, 2010; Sadagopan *et al*, 2007; Salahuddin *et al*, 1988; Bakheet *et al*, 2018).

PBs are dynamic structures that are continuously assembled and disassembled, yet relatively little is known about how they are regulated. Stimuli that activate the p38/MK2 MAP kinase pathway as well as many virus infections elicit PB disassembly and a concomitant reduction in ARE-mRNA suppression to promote inflammatory molecule production (Corcoran *et al*, 2012, 2015; Vindry *et al*, 2017; Corcoran & McCormick, 2015; Standart & Weil, 2018; Docena *et al*, 2010). We have previously shown that KSHV causes PB disassembly during latent infection, and that the viral protein Kaposin B (KapB) induces PB disassembly while enhancing the production of an ARE-containing reporter (Corcoran *et al*, 2015; Corcoran & McCormick, 2015; Corcoran *et al*, 2011). These data support the notion that PB disassembly is likely an important contributor to inflammation associated with KS (Corcoran *et al*, 2015; Wen & Damania, 2010). Although we know that KapB binds and activates the kinase MK2, and that MK2 is an important component of the mechanism of KapB-mediated PB disassembly and ARE-mRNA stabilization, we do not precisely understand how PB loss is elicited by KapB (McCormick & Ganem, 2005; Corcoran *et al*, 2015). The observation that MK2 can phosphorylate Beclin-1 to increase autophagic flux in response to nutrient scarcity (Wei *et al*, 2015) suggested to us that KapB may also drive autophagic flux. We now show that the KSHV KapB protein enhances autophagic flux, revealing an additional layer of complexity in viral regulation of autophagy during KSHV latency. We also show that KapB requires canonical autophagy machinery Atg5 and Atg14 to induce PB disassembly and ARE-mRNA stabilization and that KapB selects PB components for autophagic turnover using the selective autophagy receptor, NDP52. PB turnover is also elicited by the

mTOR inhibitor and potent autophagy inducer, Torin-1, and this process is also dependent on Atg5 and NDP52. In contrast, and despite previous observations that it elicits PB disassembly and ARE-mRNA stabilization (Corcoran *et al*, 2015), a constitutively active form of MK2 does not rely on canonical or selective autophagy machinery for PB loss. Our data reveal that cells possess both autophagy-dependent and -independent mechanisms to regulate PB turnover and inflammatory molecule production. These data also forge a new connection between the selective autophagy receptor, NDP52, and cytoplasmic PBs, both of which control innate immune responses and inflammation.

Results

KapB induces autophagic flux

KapB expression activates the stress-responsive kinase MAPKAPK2 (MK2) (McCormick & Ganem, 2005; Corcoran *et al*, 2015). Since MK2 phosphorylates the essential autophagy inducer Beclin 1 in response to amino acid starvation (Wei *et al*, 2015; Shen *et al*, 2016; Gurkar *et al*, 2013), we questioned whether KapB expression could promote autophagic flux. Essential for autophagosome expansion is the lipidation of LC3 to form LC3-II, permitting its incorporation into autophagosome membranes (Klionsky *et al*, 2012). To measure autophagic flux, we examined levels of LC3-II and the SAR, p62, with and without treatment with the lysosomal inhibitor, Bafilomycin A1 (BafA1), as both LC3-II and p62 are also substrates for autophagy (Mizushima *et al*, 2010; Mauvezin & Neufeld, 2015). To this end, human umbilical vein endothelial cells (HUVECs) were transduced with lentiviral vectors that express KapB or an empty vector control and treated for increasing times with BafA1; LC3-II and p62 accumulation in the presence or absence of BafA1 treatment was determined by immunoblotting. When KapB-expressing cells were treated for 4 h with BafA1, the amount of LC3-II and p62 increased two- and four-fold, respectively, compared to untreated cells. Both proteins showed higher accumulation after BafA1 treatment of KapB-expressing cells than equivalently treated vector controls (Fig 1A), indicating that autophagic flux was specifically enhanced in KapB-expressing cells. We also measured endogenous LC3 puncta using immunofluorescence as an indicator of autophagic flux (Kabeya, 2000; Mizushima *et al*, 2010). Untreated KapB-expressing HUVECs displayed LC3 puncta area similar to that of control cells; however, LC3 puncta area increased after BafA1 treatment, further suggesting that KapB expression enhanced autophagic flux (Fig 1B). Taken together, these data show that KapB expression induced autophagic flux in HUVECs.

Canonical autophagy is required for KapB- and Torin-mediated PB disassembly

Our group previously described that MK2 activation was an important component of KapB-mediated PB loss (Corcoran *et al*, 2015); however, these experiments did not reveal the precise mechanism of PB loss nor did they clarify if KapB was causing PB disassembly or blocking PB assembly. Since PBs are dynamic RNP granules, we wanted to determine whether KapB-mediated PB loss was a result of enhanced disassembly of PBs or prevention of their *de novo* assembly. To do so, we utilized HeLa cells that express a Dox-inducible GFP-tagged version of the PB-resident protein, Dcp1a (Youn *et al*, 2018). When fixed, GFP-positive puncta co-stain with endogenous PB proteins such as the RNA helicase DDX6/Rck and the decapping co-factor Hedls/Edc4, indicating that they represent PBs (Fig S1). KapB was transfected into these cells either before or after inducing GFP-Dcp1a granule formation. When KapB was expressed prior to granule induction, Dcp1a puncta formation was intact, although their appearance was slightly delayed compared to vector control cells (Fig S1A). However, when KapB was expressed after granule induction, GFP-positive puncta were lost (Fig S1B), indicating that KapB expression induced PB disassembly. As further evidence, we treated KapB-expressing HUVECs with sodium arsenite, a known inducer of PB assembly. We observed that sodium arsenite induced endogenous PB formation in KapB-expressing HUVECs that was indistinguishable from equivalently treated control cells (Fig S1C). Taken together, these results show that KapB expression caused PB loss by inducing PB disassembly but did not block PB assembly. We speculated that KapB may be utilizing a normal cellular pathway that mediates the turnover of RNPs, such as autophagy.

To determine if autophagy was required for KapB-mediated PB disassembly, we first inhibited autophagic flux by independently silencing two canonical autophagy genes, Atg5 and Atg14 (Fig

S2A, B). When either Atg5 or Atg14 were silenced in KapB-expressing HUVECs, PBs were restored, whereas their silencing did not have an effect in control cells (Fig 1C and D). We then examined the ability of KapB to mediate PB disassembly in Atg5 -/- MEFs, which are defective for autophagy (Katayama *et al*, 2008), as indicated by the lack of LC3-II (Fig S2C). KapB failed to disassemble PBs in Atg5 -/- MEFs but did disassemble PBs in matched wild-type controls (Fig S2D). Moreover, KapB expression resulted in a significant increase in Atg5 protein levels (Fig S2A), consistent with our other data that show that KapB is promoting autophagy. Blocking autophagic degradation with BafA1 also restored PBs in KapB-expressing cells (Fig 1E). These data suggest that KapB is accelerating PB turnover by enhancing autophagy.

Autophagy, although always occurring at a basal level, can be upregulated by many different cell stimuli including starvation or inhibition of mTOR using Torin-1, hereafter referred to as Torin (Thoreen *et al*, 2009). It was previously reported that rapamycin, an inhibitor of mTORC1, caused a loss of PBs in mammary epithelial cells (Hardy *et al*, 2017). We reasoned that if we inhibited both mTOR complexes mTORC1 and mTORC2 (Liu *et al*, 2013) using Torin, PBs would disassemble. We observed that the number of Hedls/Edc4 puncta were significantly reduced after Torin treatment, indicating that chemical induction of autophagy also resulted in the disassembly of PBs in HUVECs (Fig 2A). To ensure that Torin treatment was inducing disassembly of PBs and not preventing assembly, HUVECs were treated with sodium arsenite to induce PB formation; like KapB, Torin treatment did not prevent the assembly of PBs under stress conditions (Fig 2B). We then silenced Atg5 and tested if Torin treatment was able to disassemble PBs in these cells. Although Torin caused PB disassembly in control cells, Torin failed to alter the number of Hedls/Edc4 puncta in cells expressing shAtg5 (Fig 2C). Taken

185 together, these data show that PB turnover requires autophagy in response to both KapB and
186 Torin.

187 **Canonical autophagy is required for KapB-mediated increases in ARE-containing cytokine**
188 **transcripts**

189 PBs are nodes of mRNA regulation and microscopically visible PBs are associated with ARE-
190 mRNA decay or suppression (Guo *et al*, 2018; Luo *et al*, 2018; Corcoran *et al*, 2015, 2012;
191 Franks & Lykke-Andersen, 2008; Vindry *et al*, 2017; Blanco *et al*, 2014). We treated HUVECs
192 with conditioned media from latent KSHV-infected cells to stimulate the transcription of
193 inflammatory RNAs in a biologically relevant manner and examined levels of some endogenous
194 ARE-containing RNA transcripts in KapB-expressing cells (Fig 3A). We observed significant
195 increases of cytokine mRNA for IL-6 and IL-1β in KapB-expressing cells compared to
196 equivalently treated controls, suggesting these increases resulted from reduced transcript
197 turnover in PBs (Fig 3A). In addition, treatment with Torin promoted the enhanced steady-state
198 levels of IL-1β and COX-2 (Fig 3B), suggesting that inducing autophagy reduces turnover of
199 some ARE-mRNA transcripts. To support these findings and to simplify further studies, we
200 utilized a luciferase reporter assay that we previously developed, described in (Corcoran *et al*,
201 2011). We previously used this assay to show that KapB-mediated PB loss correlated with
202 enhanced luminescence of an ARE-containing firefly luciferase (Fluc) reporter because its rapid
203 turnover was reversed and FLuc translation was enhanced (Corcoran *et al*, 2011, 2015). Briefly,
204 HeLa cells were co-transfected with a FLuc construct containing the AU-rich element from
205 CSF2 in its 3'UTR and a Renilla luciferase (RLuc) construct with no ARE; transcription of both
206 reporter constructs was then stopped by the addition of doxycycline. In control (vector
207 transfected) cells, the FLuc-ARE mRNA decayed rapidly and FLuc luminescence relative to the

208 RLuc transfection control was low. Torin treatment caused a significant increase in FLuc/RLuc
209 relative luminescence compared to DMSO-treated control cells, supporting our RT-qPCR
210 findings (Fig 3C) and suggesting that enhanced autophagy reverses the constitutive
211 turnover/suppression of the ARE-mRNA reporter. Furthermore, KapB expression also caused a
212 significant increase in FLuc/RLuc relative luminescence compared to empty vector control cells
213 (Fig 3D) as previously shown in (Corcoran *et al*, 2015). When canonical autophagy was
214 perturbed by either Atg5 or Atg14 silencing (Fig S3A, B) KapB-expressing cells had
215 significantly decreased luminescence compared to KapB-expressing controls (Fig 3D, E).
216 Likewise, when KapB-expressing cells were treated with BafA1, relative luminescence was
217 significantly decreased compared to KapB-expressing untreated control cells (Fig 3F). Together,
218 these data showed that canonical autophagy is required for KapB-mediated increases in cytokine
219 mRNA levels and the enhanced expression of an ARE-mRNA reporter.
220

221 **Dcp1a protein levels are decreased by KapB and Torin treatment**

222 We reasoned that if KapB and Torin required autophagy for PB turnover, KapB expression or
223 Torin treatment may decrease steady-state levels of one or more key PB proteins that have
224 important scaffolding roles for granule formation, such as EDC4/Hedls, Xrn1, DDX6/Rck, or
225 Dcp1a (Ayache *et al*, 2015). Immunoblotting for these proteins revealed that steady-state levels
226 of the PB-resident protein Dcp1a were reduced in Torin-treated (Fig 4A) and KapB-expressing
227 cells (Fig 4B); however, steady-state levels of other PB-resident proteins were not affected (Fig
228 4A, C). These data suggest that autophagy induction with Torin or KapB expression promote the
229 turnover of the PB-resident protein Dcp1a, but not all PB proteins. Silencing the canonical

autophagy gene, Atg5, resulted in a reversal of KapB-mediated Dcp1a loss (Fig 4D), suggesting that autophagy is required for the loss of Dcp1a observed after KapB expression.

KapB-mediated PB disassembly and ARE-mRNA stabilization require the selective autophagy receptor NDP52

After establishing a link between KapB expression, autophagy, and PB disassembly, we wondered what specific autophagy mechanisms were at work and if selective autophagy receptors (SARs) were involved. Very little is known about how PB dynamics are regulated; however, one previous study observed the SAR, NDP52, partially co-localized with some PB proteins (Guo *et al*, 2014). For this reason, we investigated whether NDP52, p62, VCP, NBR1, or OPTN were required for KapB-mediated PB disassembly using RNA silencing. Despite trying several different shRNA sequences, our attempts to silence NBR1 were unsuccessful, and shRNAs targeting VCP resulted in significant HUVEC toxicity (Fig S4A, B). Therefore, the role of these molecules in PB turnover could not be determined in our model. Genetic knockdown of NDP52, p62, and OPTN was validated in control and KapB-expressing cells (Fig S4C-E). In these experiments, silencing of p62 or OPTN did not restore PBs in KapB-expressing cells whereas NDP52 knockdown significantly restored PBs (Fig 5A, Fig S4F). These data pinpointed an important role for NDP52 and selective autophagy in KapB-mediated PB disassembly. We then tested whether NDP52 silencing could prevent Torin-mediated PB disassembly and found that PBs could not be disassembled in cells lacking NDP52 (Fig 5B, S4G). We also examined whether these SARs were required for KapB-enhanced relative luminescence in our ARE-mRNA reporter assay. We validated silencing of NDP52, p62, and OPTN in HeLas (Fig S5A-C). Similarly, we found that p62 or OPTN knockdown had no effect on KapB-mediated FLuc/RLuc

luminescence, but NDP52 silencing decreased FLuc/RLuc luminescence compared to non-targeting, KapB-expressing controls (Fig 5C), further supporting the role of NDP52 in autophagy-mediated PB disassembly. Therefore, KapB-stimulated PB disassembly and concomitant luminescence of our ARE-containing reporter uses a mechanism dependent on NDP52.

NDP52 requires the ubiquitin-binding domain for KapB-mediated PB disassembly

NDP52 has many functions in selective autophagy and autophagosome maturation and is a crucial adaptor for mitophagy and xenophagy (Ellinghaus *et al*, 2013; Fu *et al*, 2018; Lazarou *et al*, 2015; Morriswood *et al*, 2007; Verlhac *et al*, 2015). Structural domains that are important for the function of NDP52 as a SAR include a non-canonical LC3-C interacting region (cLIR) that binds to LC3-decorated autophagosomes and a ubiquitin binding domain (UBD) that binds ubiquitinated cargo proteins, linking them to the autophagosome for engulfment (Fig 5D)
To elucidate if NDP52 was required for KapB-mediated PB disassembly because of its ability to promote selective autophagy, we performed a complementation experiment. We first silenced endogenous NDP52 in control or KapB-expressing HUVECs using shRNAs targeting the 3'UTR of NDP52 and verified its knockdown (Fig S6A). Next, NDP52 expression was restored by overexpressing a fluorescently tagged NDP52 construct. Complementation of NDP52-silenced HUVECs with wild-type NDP52 restored KapB-mediated PB disassembly compared to vector controls (Fig 5E, F; S6B, C). We next sought to determine whether the PB disassembly initiated in KapB-expressing cells was reliant on two domains of NDP52 that are important for its role as a SAR: the LIR and UBD. We restored NDP52 expression in NDP52-silenced HUVECs by complementation with a fluorescently tagged UBD mutant (C443K) or a cLIR and UBD combined mutant (V136S and C443K) (Padman *et al*, 2019; Ellinghaus *et al*, 2013; Till *et al*,

2013) (Fig 5E, F). Complementation with either of the mutated forms of NDP52 failed to restore KapB-mediated PB disassembly in NDP52-silenced HUVECs. These data indicated that the UBD of NDP52 is required for KapB-mediated PB disassembly and suggest that the LIR domain may also be important (Fig 5E, F). These data provide evidence to support that the function of NDP52 in selective autophagy is required for its role in KapB-mediated PB disassembly.

Canonical autophagy is not required for MK2-mediated PB disassembly

Because we know that KapB can directly bind and activate MK2 (McCormick & Ganem, 2005) and that MK2 is, in part, required for KapB-mediated effects on PBs and ARE-mRNA (Corcoran *et al*, 2015), we reasoned that a constitutively active version of MK2 would also induce PB disassembly in an autophagy-dependent manner. To test this, we used a phosphomimetic construct called MK2EE in which two threonine residues that are normally phosphorylated by p38 MAPK in response to stress signaling are substituted with glutamic acid residues, rendering the kinase constitutively active (Kayyali *et al*, 2002; Rousseau *et al*, 1997). We previously demonstrated that MK2EE causes PB disassembly (Corcoran *et al*, 2015) and others have shown that it can also increase autophagic flux (Wei *et al*, 2015). We confirmed that autophagy was upregulated in MK2EE-expressing HUVECs by staining for endogenous LC3 puncta. We observed that BafA1 treatment resulted in a significant increase in LC3-puncta compared to vector controls, consistent with enhanced autophagic flux (Fig 6A). Furthermore, MK2EE expression resulted in an increased accumulation of LC3-II and p62 after Baf A1 treatment to block degradation (Fig 6B). We then tested if MK2EE-induced PB disassembly was reliant on autophagic flux. MK2EE-expressing HUVECs retained the ability to disassemble PBs after Atg5 silencing (Fig 6C, S7A). MK2EE expression was previously shown to increase the FLuc/RLuc

299 relative luminescence in our reporter assay (Corcoran *et al*, 2015) and we reproduced these data
300 herein (Fig 6D). However, Atg5 silencing did not significantly decrease MK2EE-mediated
301 relative luminescence (Fig 6D, S7B). These data suggest that although MK2EE induces
302 autophagy and PB disassembly, these are unrelated phenotypes and the manner by which
303 MK2EE induces PB loss does not require canonical autophagy pathways involving Atg5.

304 Given that MK2 induces autophagy, but MK2EE-mediated PB disassembly did not require
305 canonical autophagy machinery, we speculated that MK2EE-mediated PB disassembly could be
306 facilitated by NDP52. However, p62, NDP52 and OPTN silencing did not inhibit PB
307 disassembly in MK2EE-expressing cells (Fig S7C-E; 6E; S7F). Likewise, silencing of p62,
308 OPTN, or NDP52 did not decrease FLuc/RLuc luminescence in MK2EE-expressing cells as it
309 did in KapB-expressing cells (Fig 6F, S7G-I). In fact, NDP52 knockdown increased ARE-
310 mRNA stability (Fig 6F), although the significance of this observation is unclear. These data
311 confirm that MK2-mediated PB disassembly and enhanced ARE-containing luciferase reporter
312 expression do not require canonical autophagy or selective autophagy machinery.

313

314

Discussion

Here we demonstrate that the KSHV protein, KapB, relies on selective autophagy to cause PB disassembly and enhance ARE-mRNA stability. We furthermore identified NDP52 as the selective autophagy receptor required for this process. To our knowledge, this is the first report that NDP52 regulates the turnover of endogenous PBs and the first description of the contribution of NDP52 to immune regulation by altering inflammatory cytokine RNA turnover/suppression in PBs. Our major findings are: i) KapB increases autophagic flux, thereby contributing to the complex regulation of autophagic processes during KSHV latent infection and tumourigenesis, ii) KapB-mediated PB disassembly and enhanced translation of an ARE-containing reporter requires canonical autophagy machinery and the selective autophagy receptor, NDP52, iii) Activation of autophagy by chemical inhibition of mTORC1 using Torin causes PB disassembly using a mechanism that is dependent on canonical autophagy and NDP52, suggesting that KapB manipulates an existing cellular pathway that regulates PB catabolism, and iv) the mechanism of KapB- or Torin-mediated PB disassembly differs from that induced by the constitutively active kinase, MK2 (MK2EE), which is autophagy- and NDP52-independent. These results reveal that PB turnover is mediated by autophagy-dependent and -independent mechanisms and shows that the viral KapB protein hijacks a host pathway that uses NDP52 to enhance PB catabolism and promote inflammatory molecule production.

MK2 activation promotes autophagy by phosphorylating Beclin 1 (Wei *et al*, 2015); therefore, we hypothesized that KapB, an MK2-activating viral protein (McCormick & Ganem, 2005), would utilize autophagy to promote PB clearance. Our data showed that although both KapB and MK2EE increased autophagic flux (Fig 1, Fig 6), only KapB-mediated PB disassembly required

the canonical autophagy proteins Atg5 and Atg14, and the selective autophagy protein NDP52 (Fig 1, Fig 5). MK2EE does not use an autophagy-dependent mechanism, as KapB does, for PB disassembly and our studies have not yet revealed a mechanism for PB loss in these cells. These data imply that cells employ more than one pathway to disassemble PBs, consistent with the dual mechanisms responsible for turnover of other RNP granules like stress granules (Buchan *et al*, 2013; Turakhiya *et al*, 2018). Our data also suggest that KapB hijacks both these pathways to utilize an MK2-dependent, autophagy-independent pathway and an NDP52-, autophagy-dependent pathway to disassemble PBs, suggesting the central importance of PB loss to KSHV latency. Our data are supported by previous work showing that in yeast, PB recycling requires canonical autophagy machinery, and in mammalian cells NDP52 colocalizes with a GFP-tagged version of Dcp1a when overexpressed (Buchan *et al*, 2013; Guo *et al*, 2014). We add significantly to these studies, by performing our work in primary human endothelial cells and by staining for endogenous PBs using immunofluorescence for the decapping co-factor Hedls/EDC4. We reveal that when KapB is expressed, endogenous PBs are disassembled by an Atg5-, Atg14-, and NDP52-dependent autophagy process. We also complemented NDP52-silenced cells with an shRNA-resistant NDP52. We observed the restoration of KapB-mediated PB disassembly when complementation was performed with wild-type NDP52 but not when lacking the UBD (Fig 5). These data suggest that it is the ability of NDP52 to bind ubiquitinated cargo for autophagic degradation that is required for KapB-mediated PB turnover, as has been observed in other studies on NDP52 SAR function (Xie *et al*, 2015; Cemma *et al*, 2011).

Immunoelectron microscopy showed that PBs range in size from 150 to 350 nm and possess an external area of peripheral protrusions that contain the helicase Rck/DDX6 anchored to a dense

central core of decay enzymes, including Dcp1a and Xrn1 (Cougot *et al*, 2012). Many PB-localized enzymes are required for PB stability including Dcp1a; however, only three PB proteins are required for *de novo* PB formation, DDX6, the translation suppressor, 4E-T, and LSM14a (Ayache *et al*, 2015). Our data showed that KapB expression decreased the steady-state levels of Dcp1a, while the steady-state levels of other PB proteins were unaffected (Fig 4). Inducing autophagy with the mTORC1/2 inhibitor Torin recapitulated this effect, decreasing steady-state levels of Dcp1a, but not other PB proteins (Fig 4). These data support a model where the entire PB granule is not degraded by autophagy, but PB disassembly is induced by the selective targeting of Dcp1a or another unidentified PB protein. Consistent with this, we show that PBs can still form during KapB expression if we overexpress Dcp1a-GFP or block translation using sodium arsenite (Fig S1). Dcp1a is also a target for other viruses that mediate PB disassembly; for example, infection with poliovirus also caused PB disassembly and the loss of Dcp1a over a time course of infection (Dougherty *et al*, 2011).

We do not yet understand how KapB expression or Torin treatment alters Dcp1a to promote its degradation, but we speculate that post-translational modification of Dcp1a is involved. PB proteins, including Dcp1a, EDC4/Hedls, Dcp2 and DDX6, are phosphorylated; however, the functional consequences of these phosphorylation events for PB granule formation are not yet fully appreciated (Bish *et al*, 2015; Gustafson & Wessel, 2010; Rahman *et al*, 2014; Yoon *et al*, 2010). Dcp1a is mono-phosphorylated at serine 315 which stabilizes its interaction with Dcp2; however, hyperphosphorylation of Dcp1a coincided with PB loss, showing that Dcp1a phosphorylation status regulates PB dynamics (Tenekeci *et al*, 2016; Aizer *et al*, 2013; Chiang *et al*, 2013). PB proteins including Dcp1a, Dcp2 and EDC3 are also ubiquitinated, and

manipulation of total cellular K63-ubiquitination altered PB formation and function and changed the mRNA half-life of selected cytokine transcripts in a gene-specific manner (Tenekeci *et al*, 2016). Our model is that KapB expression induces the post-translational modification of Dcp1a, or a yet to be identified PB protein, to increase its recognition by NDP52, which then targets it to nascent autophagosomes (model Fig 7). Future work will explore the interactome of NDP52 during KapB expression to determine Dcp1a post-translational modifications and whether other PB proteins are modified or targeted for degradation.

In viral cancers like KS, autophagic flux promotes a pro-tumourigenic and pro-inflammatory environment (Vescovo *et al*, 2020; Liu & Debnath, 2016; Pringle *et al*, 2019; Wu *et al*, 2012). The data shown herein brings new understanding to this complex relationship during KSHV infection. We show that KapB induces autophagic flux and NDP52 selective autophagy of PBs, thereby supporting the pro-inflammatory environment associated with latent KSHV infection and KS. The manipulation of NDP52 function and autophagic flux by KapB is yet another example of the ingenuity with which viruses usurp cellular processes; revealing a regulatory network that links NDP52 to inflammatory molecule production via PB catabolism.

Materials and Methods

Cell culture

All cells were grown at 37 °C with 5% CO_2 and 20% O_2. HEK293T cells (ATCC), HeLa Tet-Off cells (Clontech), Atg5 +/+ and -/- MEFs (Kuma *et al*, 2004), HeLa Flp-In TREx GFP-Dcp1a cells (a generous gift from Anne-Claude Gingras)(Youn *et al*, 2018), and iSLK.219 cells (a generous gift from Don Ganem) (Myoung & Ganem, 2011) were cultured in DMEM (Thermo Fisher) supplemented with 100 U/mL penicillin, 100 µg/mL streptomycin, 2 mM L-glutamine (Thermo Fisher) and 10% FBS (Thermo Fisher). iSLK.219 cells were additionally cultured in the presence of puromycin (10 µg/mL). HUVECs (Lonza) were cultured in endothelial cell growth medium (EGM-2) (Lonza). HUVECs were seeded onto gelatin (1% w/v in PBS)-coated tissue culture plates or glass coverslips. All drug treatments were performed for the times indicated in each experiment at the concentrations listed in Table 1.

Cloning

All plasmids used in this study can be found in Table 2. All shRNAs were generated by cloning shRNA hairpin sequences found in Table 3 into pLKO.1-TRC Puro (pLKO.1-TRC cloning vector was a gift from David Root (Addgene plasmid # 10878; http://n2t.net/addgene:10878; RRID:Addgene_10878) or pLKO.1-blast (pLKO.1-blast was a gift from Keith Mostov (Addgene plasmid #26655; http://n2t.net/addgene:26655; RRID:Addgene_26655). pBMN mCherry-NDP52(C443K) was a gift from Michael Lazarou (Addgene plasmid #119685; http://n2t.net/addgene:119685; RRID:Addgene_119685) and pBMN mCherry-NDP52(V136S/C443K) was a gift from Michael Lazarou (Addgene plasmid #119686; http://n2t.net/addgene:119686; RRID:Addgene_119686). The overexpression plasmids, pLJM1

mCh-NDP52 C443K and pLJM1 mCh-NDP52 C443K V136S were made using the primers in Table 4 to clone NDP52 into pLJM1 (Johnston *et al*, 2019).

Lentivirus Production and Transduction

All lentiviruses were generated using a second-generation system. Briefly, HEK293T cells were transfected with pSPAX2, MD2G, and the plasmid containing a gene of interest or hairpin using polyethylimine (PEI, Polysciences). psPAX2 was a gift from Didier Trono (Addgene plasmid #12260; http://n2t.net/addgene:12260; RRID:Addgene_12260) and pMD2.G was a gift from Didier Trono (Addgene plasmid #12259; http://n2t.net/addgene:12259; RRID:Addgene_12259).

Viral supernatants were harvested 48 h post-transfection, clarified using a 0.45 µm polyethersulfone filter (VWR), and frozen at -80°C until use. For transduction, lentiviruses were thawed at 37°C and added to target cells in complete media containing 5 µg/mL polybrene (Sigma) for 24 h. The media was changed to selection media containing 1 µg/mL puromycin or 5 µg/mL blasticidin (Thermo) and cells were selected for 48 h before proceeding with experiments.

Viral conditioned media treatment

iSLK.219 cells (latently infected with rKSHV.219 virus) (Vieira & O'Hearn, 2004) were sub-cultured into a 10 mL cell culture dish and grown without puromycin for 72 h (Myoung & Ganem, 2011). At 72 h, conditioned media was reserved and cleared of cellular debris by centrifugation at 500 x g for 5 min. Supernatant was collected and filtered through a 0.22 µm polyethersulfone (PES) membrane filter (VWR) and stored in aliquots at -80. Prior to the experiment, conditioned media was thawed at 37°C and combined 1:1 with fresh HUVEC EGM-

2 media and used to treat vector or KapB-expressing HUVECs for 0 or 6 h prior to total RNA harvest.

Immunofluorescence

Cells were seeded onto coverslips for immunofluorescence experiments and fixed for 10 mins at 37 °C in 4% (v/v) paraformaldehyde (Electron Microscopy Sciences). Samples were permeabilized with 0.1% (v/v) Triton X-100 (Sigma-Aldrich) for 10 min at room temperature and blocked in 1% human AB serum (Sigma-Aldrich) for 1 h at room temperature. For autophagosome immunofluorescence cells were fixed for 10 min in ice cold methanol at -20 °C and blocked in 1% human AB serum for 1 h at room temperature. Primary and secondary antibodies were diluted in 1% human AB serum and used at the concentrations in Table 5. Samples were mounted with Prolong Gold AntiFade mounting media (Thermo). For CellProfiler quantification of puncta, samples were incubated with WGA AlexaFluor-647 at a 1:400 dilution for 10 min prior to permeabilization. Image analysis was performed using CellProfiler (cellprofiler.org), an open source platform for image analysis (Carpenter *et al*, 2006); quantification of puncta was performed as previously described, with the exception that cells were defined by propagating out a set number of pixels from each nucleus (Castle *et al*, 2021).

Immunoblotting

Cells were lysed in 2x Laemmli buffer and stored at -20°C until use. The DC Protein Assay (Bio-Rad) was used to quantify protein concentration as per the manufacturer's instructions. 10-15 µg of protein lysate was resolved by SDS-PAGE on TGX Stain-Free acrylamide gels (BioRad). Total protein images were acquired from the PVDF membranes after transfer on the ChemiDoc Touch Imaging system (BioRad). Membranes were blocked in 5% bovine serum

albumin (BSA) or skim milk in Tris-buffered saline-Tween20 (TBS-T). Primary and secondary antibodies were diluted in 2.5% BSA or skim milk; antibody dilutions can be found in Table 5. Membranes were visualized using Clarity Western ECL substrate and the ChemiDoc Touch Imaging system (BioRad).

Luciferase Assays

Luciferase assays were performed as previously described (Corcoran *et al*, 2011). HeLa Tet-Off cells were transduced with recombinant lentivirus expressing different shRNAs and selected. Cells were transfected according to Corcoran *et al.* (2011) with pTRE2 Firefly Luciferase ARE, pTRE2 Renilla Luciferase, and the expression plasmid of interest using Fugene HD (Promega). Luciferase and renilla activity were quantified using the Dual Luciferase Assay Kit (Promega) and read on a GloMax multi-detection system (Promega).

Quantitative PCR

RNA was collected using a RNeasy Plus Mini Kit (Qiagen) according to the manufacturer's instructions and stored at -80°C until further use. RNA concentration was determined and was reverse transcribed using Maxima H Minus First Strand cDNA Synthesis Kit (Thermo Fisher) using a combination of random and oligo (dT) primers according to the manufacturer's instructions. cDNA was diluted 1:5 for all qPCR experiments and GoTaq qPCR Master Mix (Promega) was used to amplify cDNA. The ΔΔ-Quantitation cycle (Cq) method was used to determine the fold change in expression of target transcripts. qPCR primer sequences can be found in Table 6.

Statistics

Data shown are the mean ± standard error of the mean (SEM). Statistical significance was determined using a one-way ANOVA, a 2-way ANOVA or Student's t-test when appropriate with the applicable post-test (indicated in the corresponding figure legends). For ANOVAs, matched data from each replicate was paired for analysis. All statistics were performed using GraphPad Prism v.9.0.

Acknowledgements

The authors would like to dedicate this manuscript to Dr. Beth Levine, who was a leader in the field of autophagy and viruses and who inspired this work. We sincerely thank the members of the Corcoran lab for helpful discussions about this work. We would like to thank Dr. Craig McCormick (Dalhousie University), Dr. Eric Pringle (Dalhousie University), and Dr. Andrew Leidal (UCSF) for valuable feedback on this manuscript and the McCormick lab for plasmids, expertise and advice. We would like to thank Mr. Stephen Whitefield and Ms. Mary Ann Trevors in the Dalhousie *CORES* (Cellular and Molecular Digital Imaging and Electron Microscopy core facilities) and Dr. Anne Vaahtokari of the Charbonneau Microscopy Facility, UCalgary for microscopy support. We would like to thank Dr. Andreas Till (University of Bonn), Dr. Anne-Claude Gingras (Lunenfeld-Tanenbaum Research Institute) and Dr. Don Ganem (Novartis) for sharing valuable reagents. Model figure created with BioRender. GKS was supported by a CIHR CGS-M scholarship and Scotia Scholars NSHRF graduate training award. ELC was supported by a Killam predoctoral scholarship, an NSERC CGS-M scholarship, and a Nova Scotia Graduate scholarship. Operating funds to support this work derive from a CIHR Project Grant PJT-153210 to JAC.

Author Contributions

Carolyn-Ann Robinson: Conceptualization, Experimentation, Analysis, Paper Writing

Gillian K. Singh: Conceptualization, Experimentation, Analysis, Paper Writing

Elizabeth L. Castle: Analysis

Bre Q. Boudreau: Experimentation

Jennifer A. Corcoran: Conceptualization, Experimentation, Supervision, Funding Acquisition, Project Administration, Paper Writing

Conflict of Interest

The authors have no competing interests to declare.

References

Ahmad L, Mostowy S & Sancho-Shimizu V (2018) Autophagy-virus interplay: From cell biology to human disease. *Front Cell Dev Biol* 6 doi:10.3389/fcell.2018.00155 [PREPRINT]

Aizer A, Kafri P, Kalo A & Shav-Tal Y (2013) The P Body Protein Dcp1a Is Hyper-phosphorylated during Mitosis. *PLoS One* 8: e49783

Ayache J, Bénard M, Ernoult-Lange M, Minshall N, Standart N, Kress M & Weil D (2015) P-body assembly requires DDX6 repression complexes rather than decay or Ataxin2/2L complexes. *Mol Biol Cell* 26: 2579–2595

Bakheet T, Hitti E & Khabar KSA (2018) ARED-Plus: An updated and expanded database of AU-rich element-containing mRNAs and pre-mRNAs. *Nucleic Acids Res* 46: D218–D220

Balgi AD, Fonseca BD, Donohue E, Tsang TCF, Lajoie P, Proud CG, Nabi IR & Roberge M (2009) Screen for chemical modulators of autophagy reveals novel therapeutic inhibitors of mTORC1 signaling. *PLoS One* 4

Barreau C, Paillard L & Osborne HB (2005) AU-rich elements and associated factors: Are there unifying principles? *Nucleic Acids Res* 33: 7138–7150 doi:10.1093/nar/gki1012 [PREPRINT]

Birgisdottir ÅB, Lamark T & Johansen T (2013) The LIR motif - crucial for selective autophagy. *J Cell Sci* 126: 3237–47

Bish R, Cuevas-Polo N, Cheng Z, Hambardzumyan D, Munschauer M, Landthaler M & Vogel C (2015) Comprehensive Protein Interactome Analysis of a Key RNA Helicase: Detection of Novel Stress Granule Proteins. *Biomolecules* 5: 1441–66

Blanco FF, Sanduja S, Deane NG, Blackshear PJ & Dixon D a (2014) Transforming growth factor β regulates P-body formation through induction of the mRNA decay factor tristetraprolin. *Mol Cell Biol* 34: 180–95

Broussard G & Damania B (2020) Regulation of KSHV Latency and Lytic Reactivation. *Viruses* 12 doi:10.3390/v12091034 [PREPRINT]

Buchan JR, Kolaitis R, Taylor JP & Parker R (2013) Eukaryotic Stress Granules Are Cleared by Autophagy and Cdc48 / VCP Function. *Cell* 153: 1461–1474

Carpenter AE, Jones TR, Lamprecht MR, Clarke C, Kang I, Friman O, Guertin DA, Chang J, Lindquist RA, Moffat J, *et al* (2006) CellProfiler: image analysis software for identifying and quantifying cell phenotypes. *Genome Biol* 7: R100

Castle EL, Robinson C-A, Douglas P, Rinker KD & Corcoran JA (2021) Viral manipulation of a mechanoresponsive signaling axis disassembles processing bodies. *bioRxiv*: 2020.05.15.091876

Cemma M, Kim PK & Brumell JH (2011) The ubiquitin-binding adaptor proteins p62/SQSTM1 and NDP52 are recruited independently to bacteria-associated microdomains to target

561 Salmonella to the autophagy pathway. *Autophagy* 7: 341–5

562 Cesarman E, Chang Y, Moore PS, Said JW & Knowles DM (1995) Kaposi's sarcoma-associated
563 herpesvirus-like DNA sequences in AIDS-related body-cavity-based lymphomas. *N Engl J*
564 *Med* 332: 1186–1191

565 Chang Y, Cesarman E, Pessin MS, Lee F, Culpepper J, Knowles DM & Moore PS (1994)
566 Identification of herpesvirus-like DNA sequences in AIDS-associated Kaposi's sarcoma.
567 *Science* 266: 1865–9

568 Chen M, Meng Q, Qin Y, Liang P, Tan P, He L, Zhou Y, Chen Y, Huang J, Wang RF, *et al*
569 (2016) TRIM14 Inhibits cGAS Degradation Mediated by Selective Autophagy Receptor
570 p62 to Promote Innate Immune Responses. *Mol Cell* 64: 105–119

571 Chiang PY, Shen YF, Su YL, Kao CH, Lin NY, Hsu PH, Tsai MD, Wang SC, Chang GD, Lee
572 SC, *et al* (2013) Phosphorylation of mRNA Decapping Protein Dcp1a by the ERK
573 Signaling Pathway during Early Differentiation of 3T3-L1 Preadipocytes. *PLoS One* 8

574 Corbet GA & Parker R (2019) RNP granule formation: Lessons from P-bodies and stress
575 granules. *Cold Spring Harb Symp Quant Biol* 84: 203–215

576 Corcoran JA, Johnston BP & McCormick C (2015) Viral activation of MK2-hsp27-
577 p115RhoGEF-RhoA signaling axis causes cytoskeletal rearrangements, p-body disruption
578 and ARE-mRNA stabilization. *PLoS Pathog* 11: e1004597

579 Corcoran JA, Khaperskyy DA, Johnston BP, King CA, Cyr DP, Olsthoorn A V. & McCormick
580 C (2012) Kaposi's Sarcoma-Associated Herpesvirus G-Protein-Coupled Receptor Prevents
581 AU-Rich-Element-Mediated mRNA Decay. *J Virol* 86: 8859–8871

582 Corcoran JA, Khaperskyy DA & McCormick C (2011) Assays for monitoring viral manipulation
583 of host ARE-mRNA turnover. *Methods* 55: 172–181

584 Corcoran JA & McCormick C (2015) Viral activation of stress-regulated Rho-GTPase signaling
585 pathway disrupts sites of mRNA degradation to influence cellular gene expression. *Small*
586 *GTPases* 6: 178–185 doi:10.1080/21541248.2015.1093068 [PREPRINT]

587 Cougot N, Cavalier A, Thomas D & Gillet R (2012) The Dual Organization of P-bodies
588 Revealed by Immunoelectron Microscopy and Electron Tomography. *J Mol Biol* 420: 17–
589 28

590 Decker LL, Shankar P, Khan G, Freeman RB, Dezube BJ, Lieberman J & Thorley-Lawson DA
591 (1996) The Kaposi sarcoma-associated herpesvirus (KSHV) is present as an intact latent
592 genome in KS tissue but replicates in the peripheral blood mononuclear cells of KS patients.
593 *J Exp Med* 184: 283–8

594 Docena G, Rovedatti L, Kruidenier L, Fanning Á, Leakey NAB, Knowles CH, Lee K, Shanahan
595 F, Nally K, McLean PG, *et al* (2010) Down-regulation of p38 mitogen-activated protein
596 kinase activation and proinflammatory cytokine production by mitogen-activated protein
597 kinase inhibitors in inflammatory bowel disease. *Clin Exp Immunol* 162: 108–115

598 Dougherty JD, White JP & Lloyd RE (2011) Poliovirus-mediated disruption of cytoplasmic
599 processing bodies. *J Virol* 85: 64–75

Du Y, Duan T, Feng Y, Liu Q, Lin M, Cui J & Wang R (2018) LRRC25 inhibits type I IFN signaling by targeting ISG15-associated RIG-I for autophagic degradation. *EMBO J* 37: 351–366

Dunn WA, Cregg JM, Kiel JAKW, van der Klei IJ, Oku M, Sakai Y, Sibirny AA, Stasyk O V. & Veenhuis M (2005) Pexophagy: the selective autophagy of peroxisomes. *Autophagy* 1: 75–83 doi:10.4161/auto.1.2.1737 [PREPRINT]

Ellinghaus D, Zhang H, Zeissig S, Lipinski S, Till A, Jiang T, Stade B, Bromberg Y, Ellinghaus E, Keller A, *et al* (2013) Association between variants of PRDM1 and NDP52 and Crohn's disease, based on exome sequencing and functional studies. *Gastroenterology* 145: 339–47

Ensoli B, Nakamura S, Salahuddin SZ, Biberfeld P, Larsson L, Beaver B, Wong-staal F & Gallo RC (2010) AIDS-Kaposi's Sarcoma-Derived Cells Express Cytokines with Autocrine and Paracrine Growth Effects. *Science (80-)* 243: 223–226

Ensoli B & Stürzl M (1998) Kaposi's sarcoma: a result of the interplay among inflammatory cytokines, angiogenic factors and viral agents. *Cytokine Growth Factor Rev* 9: 63–83

Franks TM & Lykke-Andersen J (2007) TTP and BRF proteins nucleate processing body formation to silence mRNAs with AU-rich elements. *Genes Dev* 21: 719–735

Franks TM & Lykke-Andersen J (2008) The control of mRNA decapping and P-body formation. *Mol Cell* 32: 605–15

Fu T, Liu J, Wang Y, Xie X, Hu S & Pan L (2018) Mechanistic insights into the interactions of NAP1 with the SKICH domains of NDP52 and TAX1BP1. *Proc Natl Acad Sci U S A* 115: E11651–E11660

García-Mauriño SM, Rivero-Rodríguez F, Velázquez-Cruz A, Hernández-Vellisca M, Díaz-Quintana A, De la Rosa MA & Díaz-Moreno I (2017) RNA binding protein regulation and cross-talk in the control of AU-rich mRNA Fate. *Front Mol Biosci* 4: 71 doi:10.3389/fmolb.2017.00071 [PREPRINT]

Green DR, Galluzzi L & Kroemer G (2011) Mitochondria and the autophagy-inflammation-cell death axis in organismal aging. *Science (80-)* 333: 1109–1112 doi:10.1126/science.1201940 [PREPRINT]

Guo H, Chitiprolu M, Gagnon D, Meng L, Perez-Iratxeta C, Lagace D & Gibbings D (2014) Autophagy supports genomic stability by degrading retrotransposon RNA. *Nat Commun* 5: 5276

Guo L, Louis IV-S & Bohjanen PR (2018) Post-transcriptional regulation of cytokine expression and signaling. *Curr Trends Immunol* 19: 33–40

Gurkar AU, Chu K, Raj L, Bouley R, Lee S-H, Kim Y-B, Dunn SE, Mandinova A & Lee SW (2013) Identification of ROCK1 kinase as a critical regulator of Beclin1-mediated autophagy during metabolic stress. *Nat Commun* 4: 2189

Gustafson EA & Wessel GM (2010) DEAD-box helicases: posttranslational regulation and function. *Biochem Biophys Res Commun* 395: 1–6

638 Hardy SD, Shinde A, Wang W-H, Wendt MK & Geahlen RL (2017) Regulation of epithelial-
639 mesenchymal transition and metastasis by TGF-β, P-bodies, and autophagy. *Oncotarget* 8:
640 103302–103314

641 He X, Zhu Y, Zhang Y, Geng Y, Gong J, Geng J, Zhang P, Zhang X, Liu N, Peng Y, *et al* (2019)
642 RNF 34 functions in immunity and selective mitophagy by targeting MAVS for autophagic
643 degradation . *EMBO J* 38

644 Hubstenberger A, Courel M, Bénard M, Souquere S, Ernoult-Lange M, Chouaib R, Yi Z, Morlot
645 J-B, Munier A, Fradet M, *et al* (2017) P-Body Purification Reveals the Condensation of
646 Repressed mRNA Regulons. *Mol Cell* 68: 144-157.e5

647 Ichimura Y, Kumanomidou T, Sou Y, Mizushima T, Ezaki J, Ueno T, Kominami E, Yamane T,
648 Tanaka K & Komatsu M (2008) Structural basis for sorting mechanism of p62 in selective
649 autophagy. *J Biol Chem* 283: 22847–57

650 Jin S, Tian S, Luo M, Xie W, Liu T, Duan T, Wu Y & Cui J (2017) Tetherin Suppresses Type I
651 Interferon Signaling by Targeting MAVS for NDP52-Mediated Selective Autophagic
652 Degradation in Human Cells. *Mol Cell* 68: 308-322.e4

653 Johnston BP, Pringle ES & McCormick C (2019) KSHV activates unfolded protein response
654 sensors but suppresses downstream transcriptional responses to support lytic replication.
655 *PLoS Pathog* 15

656 Kabeya Y (2000) LC3, a mammalian homologue of yeast Apg8p, is localized in autophagosome
657 membranes after processing. *EMBO J* 19: 5720–5728

658 Katayama H, Yamamoto A, Mizushima N, Yoshimori T & Miyawaki A (2008) GFP-like
659 proteins stably accumulate in lysosomes. *Cell Struct Funct* 33: 1–12

660 Kayyali US, Pennella CM, Trujillo C, Villa O, Gaestel M & Hassoun PM (2002) Cytoskeletal
661 changes in hypoxic pulmonary endothelial cells are dependent on MAPK-activated protein
662 kinase MK2. *J Biol Chem* 277: 42596–42602

663 Kenific CM, Stehbens SJ, Goldsmith J, Leidal AM, Faure N, Ye J, Wittmann T & Debnath J
664 (2016) NBR 1 enables autophagy-dependent focal adhesion turnover. *J Cell Biol* 212: 577–
665 590

666 Klionsky DJ, Abdalla FC, Abeliovich H, Abraham RT, Acevedo-Arozena A, Adeli K, Agholme
667 L, Agnello M, Agostinis P, Aguirre-Ghiso JA, *et al* (2012) Guidelines for the use and
668 interpretation of assays for monitoring autophagy. *Autophagy* 8: 445–544

669 Kuma A, Hatano M, Matsui M, Yamamoto A, Nakaya H, Yoshimori T, Ohsumi Y, Tokuhisa T
670 & Mizushima N (2004) The role of autophagy during the early neonatal starvation period.
671 *Nature* 432: 1032–1036

672 Lai WS & Blackshear PJ (2001) Interactions of CCCH zinc finger proteins with mRNA.
673 Tristetraprolin-mediated AU-rich element-dependent mRNA degradation can occur in the
674 absence of a poly(A) tail. *J Biol Chem* 276: 23144–23154

675 Lai WS, Carballo E, Strum JR, Kennington EA, Phillips RS & Blackshear PJ (1999) Evidence
676 that Tristetraprolin Binds to AU-Rich Elements and Promotes the Deadenylation and

677 Destabilization of Tumor Necrosis Factor Alpha mRNA. *Mol Cell Biol* 19: 4311–4323

678 Lane BR, Liu J, Bock PJ, Schols D, Coffey MJ, Strieter RM, Polverini PJ & Markovitz DM
679 (2002) Interleukin-8 and growth-regulated oncogene alpha mediate angiogenesis in
680 Kaposi's sarcoma. *J Virol* 76: 11570–83

681 Lazarou M, Sliter DA, Kane LA, Sarraf SA, Wang C, Burman JL, Sideris DP, Fogel AI & Youle
682 RJ (2015) The ubiquitin kinase PINK1 recruits autophagy receptors to induce mitophagy.
683 *Nature* 524: 309–314

684 Lee J-S, Li Q, Lee J-Y, Lee S-H, Jeong JH, Lee H-R, Chang H, Zhou F-C, Gao S-J, Liang C, *et*
685 *al* (2009) FLIP-mediated autophagy regulation in cell death control. *Nat Cell Biol* 11: 1355–
686 1362

687 Leidal AM, Cyr DP, Hill RJ, Lee PWK & McCormick C (2012) Subversion of autophagy by
688 Kaposi's sarcoma-associated herpesvirus impairs oncogene-induced senescence. *Cell Host*
689 *Microbe* 11: 167–180

690 Levine B, Sinha S & Kroemer G (2008) Bcl-2 family members: Dual regulators of apoptosis and
691 autophagy. *Autophagy* 4: 600–606 doi:10.4161/auto.6260 [PREPRINT]

692 Liu J & Debnath J (2016) The Evolving, Multifaceted Roles of Autophagy in Cancer. In
693 *Advances in Cancer Research* pp 1–53. Academic Press Inc.

694 Liu Q, Xu C, Kirubakaran S, Zhang X, Hur W, Liu Y, Kwiatkowski NP, Wang J, Westover KD,
695 Gao P, *et al* (2013) Characterization of Torin2, an ATP-competitive inhibitor of mTOR,
696 ATM, and ATR. *Cancer Res* 73: 2574–2586

697 Luo Y, Na Z & Slavoff SA (2018) P-Bodies: Composition, Properties, and Functions.
698 *Biochemistry* 57: 2424

699 Maitra S, Chou CF, Luber CA, Lee KY, Mann M & Chen CY (2008) The AU-rich element
700 mRNA decay-promoting activity of BRF1 is regulated by mitogen-activated protein kinase-
701 activated protein kinase 2. *RNA* 14: 950–959

702 Maiuri MC & Kroemer G (2015) Autophagy in stress and disease. *Cell Death Differ* 22: 365–
703 366 doi:10.1038/cdd.2014.236 [PREPRINT]

704 Mauvezin C & Neufeld TP (2015) Bafilomycin A1 disrupts autophagic flux by inhibiting both
705 V-ATPase-dependent acidification and Ca-P60A/SERCA-dependent autophagosome-
706 lysosome fusion. *Autophagy* 11: 1437–1438

707 McCormick C & Ganem D (2005) The Kaposin B Protein of KSHV Activates the p38/MK2
708 Pathway and Stabilizes Cytokine mRNAs. *Science (80-)* 307: 739–741

709 Miles SA, Rezai AR, Salazar-González JF, Vander Meyden M, Stevens RH, Logan DM,
710 Mitsuyasu RT, Taga T, Hirano T & Kishimoto T (1990) AIDS Kaposi sarcoma-derived
711 cells produce and respond to interleukin 6. *Proc Natl Acad Sci U S A* 87: 4068–72

712 Mizushima N, Yoshimori T & Levine B (2010) Methods in Mammalian Autophagy Research.
713 *Cell* 140: 313–326 doi:10.1016/j.cell.2010.01.028 [PREPRINT]

714 Mohamud Y, Qu J, Xue YC, Liu H, Deng H & Luo H (2019) CALCOCO2/NDP52 and

SQSTM1/p62 differentially regulate coxsackievirus B3 propagation. *Cell Death Differ* 26: 1062–1076

Morishita H & Mizushima N (2019) Diverse cellular roles of autophagy. *Annu Rev Cell Dev Biol* 35: 453–475 doi:10.1146/annurev-cellbio-100818-125300 [PREPRINT]

Morriswood B, Ryzhakov G, Puri C, Arden SD, Roberts R, Dendrou C, Kendrick-Jones J & Buss F (2007) T6BP and NDP52 are myosin VI binding partners with potential roles in cytokine signalling and cell adhesion. *J Cell Sci* 120: 2574–85

Myoung J & Ganem D (2011) iSLK cell. *J Virol Methods* 174: 12–21

Noda NN, Kumeta H, Nakatogawa H, Satoo K, Adachi W, Ishii J, Fujioka Y, Ohsumi Y & Inagaki F (2008) Structural basis of target recognition by Atg8/LC3 during selective autophagy. *Genes to Cells* 13: 1211–1218

Noda NN, Ohsumi Y & Inagaki F (2010) Atg8-family interacting motif crucial for selective autophagy. *FEBS Lett* 584: 1379–1385

Padman BS, Nguyen TN, Uoselis L, Skulsuppaisarn M, Nguyen LK & Lazarou M (2019) LC3/GABARAPs drive ubiquitin-independent recruitment of Optineurin and NDP52 to amplify mitophagy. *Nat Commun* 10: 1–13

Prabakaran T, Bodda C, Krapp C, Zhang B, Christensen MH, Sun C, Reinert L, Cai Y, Jensen SB, Skouboe MK, *et al* (2018) Attenuation of c GAS - STING signaling is mediated by a p62/ SQSTM 1-dependent autophagy pathway activated by TBK1 . *EMBO J* 37

Pringle ES, Robinson C-A & McCormick C (2019) Kaposi's Sarcoma-Associated Herpesvirus Lytic Replication Interferes with mTORC1 Regulation of Autophagy and Viral Protein Synthesis. *J Virol* 93

Rahman H, Qasim M, Oellerich M & Asif AR (2014) Crosstalk between Edc4 and mammalian target of rapamycin complex 1 (mTORC1) signaling in mRNA decapping. *Int J Mol Sci* 15: 23179–95

Riggs CL, Kedersha N, Ivanov P & Anderson P (2020) Mammalian stress granules and P bodies at a glance. *J Cell Sci* 133 doi:10.1242/jcs.242487 [PREPRINT]

Riva G, Barozzi P, Torelli G & Luppi M (2010) Immunological and Inflammatory Features of Kaposi's Sarcom and Other Kaposi's Sarcoma-Associated Herpesvirus/Human Herpesvirus 8-Associated Neoplasias. *AIDS Rev* 9: 25–39

Rogov V, Dötsch V, Johansen T & Kirkin V (2014) Interactions between Autophagy Receptors and Ubiquitin-like Proteins Form the Molecular Basis for Selective Autophagy. *Mol Cell* 53: 167–178

Rousseau S, Houle F, Landry J & Huot J (1997) P38 MAP kinase activation by vascular endothelial growth factor mediates actin reorganization and cell migration in human endothelial cells. *Oncogene* 15: 2169–2177

Sadagopan S, Sharma-Walia N, Veettil MV, Raghu H, Sivakumar R, Bottero V & Chandran B (2007) Kaposi's Sarcoma-Associated Herpesvirus Induces Sustained NF-κB Activation

753 during De Novo Infection of Primary Human Dermal Microvascular Endothelial Cells That
754 Is Essential for Viral Gene Expression. *J Virol* 81: 3949–3968

755 Salahuddin S, Nakamura S, Biberfeld P, Kaplan M, Markham P, Larsson L & Gallo R (1988)
756 Angiogenic properties of Kaposi's sarcoma-derived cells after long-term culture in vitro.
757 *Science (80-)* 242: 430–433

758 Sargsyan A, Cai J, Fandino LB, Labasky ME, Forostyan T, Colosimo LK, Thompson SJ &
759 Graham TE (2015) Rapid parallel measurements of macroautophagy and mitophagy in
760 mammalian cells using a single fluorescent biosensor. *Sci Rep* 5

761 Seth RB, Sun L, Ea CK & Chen ZJ (2005) Identification and characterization of MAVS, a
762 mitochondrial antiviral signaling protein that activates NF-κB and IRF3. *Cell* 122: 669–682

763 Shen L, Qi Z, Zhu Y, Song X, Xuan C, Ben P, Lan L, Luo L & Yin Z (2016) Phosphorylated
764 heat shock protein 27 promotes lipid clearance in hepatic cells through interacting with
765 STAT3 and activating autophagy. *Cell Signal* 28: 1086–1098

766 Soulier J, Grollet L, Oksenhendler E, Cacoub P, Cazals-Hatem D, Babinet P, d'Agay MF,
767 Clauvel JP, Raphael M & Degos L (1995) Kaposi's sarcoma-associated herpesvirus-like
768 DNA sequences in multicentric Castleman's disease. *Blood* 86: 1276–80

769 Standart N & Weil D (2018) P-Bodies: Cytosolic Droplets for Coordinated mRNA Storage.
770 *Trends Genet* 34: 612–626 doi:10.1016/j.tig.2018.05.005 [PREPRINT]

771 Staskus KA, Zhong W, Gebhard K, Herndier B, Wang H, Renne R, Beneke J, Pudney J,
772 Anderson DJ, Ganem D, *et al* (1997) Kaposi's sarcoma-associated herpesvirus gene
773 expression in endothelial (spindle) tumor cells. *J Virol* 71: 715–9

774 Sumpter R & Levine B (2011) Selective autophagy and viruses. *Autophagy* 7: 260–265
775 doi:10.4161/auto.7.3.14281 [PREPRINT]

776 Tenekeci U, Poppe M, Beuerlein K, Busch J, Schmitz ML & Kracht Correspondence M (2016)
777 K63-Ubiquitylation and TRAF6 Pathways Regulate Mammalian P-Body Formation and
778 mRNA Decapping. *Mol Cell* 62: 943–957

779 Thoreen CC, Kang SA, Won Chang J, Liu Q, Zhang J, Gao Y, Reichling LJ, Sim T, Sabatini DM
780 & Gray NS (2009) An ATP-competitive Mammalian Target of Rapamycin Inhibitor
781 Reveals Rapamycin-resistant Functions of mTORC1 * □ S. *J Biol Chem* 284: 8023–32

782 Till A, Lipinski S, Ellinghaus D, Mayr G, Subramani S, Rosenstiel P & Franke A (2013)
783 Autophagy receptor CALCOCO2/NDP52 takes center stage in Crohn disease. *Autophagy* 9:
784 1256–7

785 Tripathi DN, Zhang J, Jing J, Dere R & Walker CL (2016) A new role for ATM in selective
786 autophagy of peroxisomes (pexophagy). *Autophagy* 12: 711–712
787 doi:10.1080/15548627.2015.1123375 [PREPRINT]

788 Turakhiya A, Meyer SR, Marincola G, Böhm S, Vanselow JT, Schlosser A, Hofmann K &
789 Buchberger A (2018) ZFAND1 Recruits p97 and the 26S Proteasome to Promote the
790 Clearance of Arsenite-Induced Stress Granules. *Mol Cell* 70: 906-919.e7

Verlhac P, Gré IP, Viret C & Faure M (2015) Autophagy Receptor NDP52 Regulates Pathogen-Containing Autophagosome Maturation. *Cell Host Microbe* 17: 515–525

Vescovo T, Pagni B, Piacentini M, Fimia GM & Antonioli M (2020) Regulation of Autophagy in Cells Infected With Oncogenic Human Viruses and Its Impact on Cancer Development. *Front Cell Dev Biol* 8 doi:10.3389/fcell.2020.00047 [PREPRINT]

Vieira J & O'Hearn PM (2004) Use of the red fluorescent protein as a marker of Kaposi's sarcoma-associated herpesvirus lytic gene expression. *Virology* 325: 225–240

Vindry C, Marnef A, Broomhead H, Twyffels L, Ozgur S, Stoecklin G, Llorian M, Smith CW, Mata J, Weil D, *et al* (2017) Dual RNA Processing Roles of Pat1b via Cytoplasmic Lsm1-7 and Nuclear Lsm2-8 Complexes. *Cell Rep* 20: 1187–1200

Wei Y, An Z, Zou Z, Sumpter R, Su M, Zang X, Sinha S, Gaestel M & Levine B (2015) The stress-responsive kinases MAPKAPK2/MAPKAPK3 activate starvation-induced autophagy through Beclin 1 phosphorylation. *Elife* 4

Wen KW & Damania B (2010) Kaposi sarcoma-associated herpesvirus (KSHV): molecular biology and oncogenesis. *Cancer Lett* 289: 140–50

Wu WKK, Coffelt SB, Cho CH, Wang XJ, Lee CW, Chan FKL, Yu J & Sung JJY (2012) The autophagic paradox in cancer therapy. *Oncogene* 31: 939–953 doi:10.1038/onc.2011.295 [PREPRINT]

Wu Y, Jin S, Liu Q, Zhang Y, Ma L, Zhao Z, Yang S, Li YP & Cui J (2020) Selective autophagy controls the stability of transcription factor IRF3 to balance type I interferon production and immune suppression. *Autophagy*

Xie X, Li F, Wang Y, Wang Y, Lin Z, Cheng X, Liu J, Chen C & Pan L (2015) Molecular basis of ubiquitin recognition by the autophagy receptor CALCOCO2. *Autophagy* 11: 1775–89

Yang Q, Liu TT, Lin H, Zhang M, Wei J, Luo WW, Hu YH, Zhong B, Hu MM & Shu HB (2017) TRIM32-TAX1BP1-dependent selective autophagic degradation of TRIF negatively regulates TLR3/4-mediated innate immune responses. *PLoS Pathog* 13

Yao Z & Klionsky DJ (2016) An unconventional pathway for mitochondrial protein degradation. *Autophagy* 12: 1971–1972 doi:10.1080/15548627.2016.1235127 [PREPRINT]

Yoon J-H, Choi E-J & Parker R (2010) Dcp2 phosphorylation by Ste20 modulates stress granule assembly and mRNA decay in Saccharomyces cerevisiae. *J Cell Biol* 189: 813–27

Youn JY, Dunham WH, Hong SJ, Knight JDR, Bashkurov M, Chen GI, Bagci H, Rathod B, MacLeod G, Eng SWM, *et al* (2018) High-Density Proximity Mapping Reveals the Subcellular Organization of mRNA-Associated Granules and Bodies. *Mol Cell* 69: 517-532.e11

Young ARJ, Narita M, Ferreira M, Kirschner K, Sadaie M, Darot JFJ, Tavaré S, Arakawa S, Shimizu S, Watt FM, *et al* (2009) Autophagy mediates the mitotic senescence transition. *Genes Dev* 23: 798–803

Zaffagnini G & Martens S (2016) Mechanisms of Selective Autophagy. *J Mol Biol* 428: 1714–

829 1724

830

831

Figure Legends

Figure 1: Kaposin B requires canonical autophagy to disassemble PBs. Primary human umbilical vein endothelial cells (HUVECs) were transduced with recombinant lentiviruses expressing either Kaposin B (KapB) or an empty vector control and selected with blasticidin (5 µg/mL). A: Cells were treated with bafilomycin A1 (10 nM) or a vehicle control (DMSO) for the indicated times prior to harvest in 2x Laemmli buffer. Protein lysates were resolved by SDS-PAGE and immunoblot was performed for p62 and LC3. Samples were quantified using Image Lab (Biorad) software and then normalized, first to total protein and then to their respective starting time points (0 h). Results were plotted in GraphPad and a linear regression statistical test was performed, ±SEM; n=3, *=P<0.05, ***=P<0.001. B: Cells were treated with BafA1 for 30 min prior to fixation in methanol. Immunofluorescence was performed for LC3 (white) and DAPI (nuclei, blue). Scale bar=20 µm. Total LC3 area per field was quantified by identifying LC3-positive puncta using CellProfiler and normalizing to the number of nuclei and the vector DMSO control. Results were plotted in GraphPad, a 2-way ANOVA was performed with a Šidák's multiple comparison test, ±SEM; n=3, *=P<0.05. C: HUVECs were sequentially transduced: first with recombinant lentiviruses expressing either shRNAs targeting Atg5 or Atg14 (shAtg5, shAtg14) or a non-targeting control (NS) and selected with puromycin (1 µg/mL), and second with either KapB or an empty vector control and selected with blasticidin (5 µg/mL). Coverslips were fixed in 4% paraformaldehyde, permeabilized in 0.1% Triton X-100, and immunostained for the PB-resident protein Hedls (white) and nuclei (DAPI). Scale bar=20 µm. Hedls puncta were quantified using CellProfiler and normalized to the number of nuclei, results were plotted in GraphPad and a 2-way ANOVA was performed with a Šidák's multiple comparison test, ±SEM; n=3, *=P<0.05. D: HUVECs were transduced as in A and treated with

DMSO or bafilomycin A1 (10 nM) for 30 min before being fixed in 4% paraformaldehyde and permeabilized in 0.1% Triton X-100. Immunofluorescence was performed for Hedls (PBs, white) and DAPI (nuclei, blue). Scale bar=20 µm. Hedls puncta were counted using CellProfiler and normalized to the number of nuclei, results were plotted in GraphPad and a 2-way ANOVA was performed with a Šidák's multiple comparison test, ±SEM; n=3, *=P<0.05.

Figure 2: Torin treatment disassembles PBs. A: HUVECs were treated with either Torin (250 nM) or a DMSO control for 2 h prior to fixation in 4% paraformaldehyde. Samples were permeabilized in 0.1% Triton X-100. Immunofluorescence was performed for Hedls (PBs, white) and DAPI (nuclei, blue). Scale bar=20 µm. Hedls puncta were counted using CellProfiler and normalized to the number of nuclei, results were plotted in GraphPad and a 2-way ANOVA was performed with a Šidák's multiple comparison test, ±SEM; n=3, *=P<0.05. B: HUVECs were treated with either Torin (250 nM) or a DMSO control for 90 min prior to the addition of sodium arsenite (0.25 mM) for 30 min. Cells were fixed in 4% paraformaldehyde and permeabilized in 0.1% Triton X-100. Immunofluorescence was performed for Hedls (PBs, white) and DAPI (nuclei, blue). Scale bar=20 µm. C: HUVECs were transduced with recombinant lentiviruses expressing either shRNAs targeting Atg5 (shAtg5) or a non-targeting control (NS) and selected with puromycin (1 µg/mL). Cells were treated with Torin (250 nM) or DMSO for 2 h prior to fixation in in 4% paraformaldehyde and permeabilization in 0.1% Triton X-100. Samples were immunostained for the PB-resident protein Hedls (white) and nuclei (DAPI). Scale bar=20 µm. Hedls puncta were quantified using CellProfiler and normalized to the number of nuclei, results were plotted in GraphPad and a 2-way ANOVA was performed with a Šidák's multiple comparison test, ±SEM; n=4, *=P<0.05.

Figure 3: KapB-mediated ARE-mRNA reporter expression requires canonical autophagy. A: HUVECs were transduced with recombinant lentiviruses expressing either KapB or an empty vector control and selected with blasticidin (5 µg/mL). Conditioned media harvested from KSHV latently infected cells was used to mimic the KS lesion microenvironment and induce the transcription of cytokines for 6 h prior to lysis for total RNA, normal media was used for the 0 h time point. Transcript levels were quantified by qPCR and normalized to 18S as a reference gene. Data is represented as the fold change in target transcript expression relative to the untreated vector control and was quantified using the ΔΔCq method. Results were plotted in GraphPad, a 2-way ANOVA was performed, ±SEM; n=3, *=P<0.05, **=P<0.01. B: HUVECs were treated with Torin (250 nM) or a DMSO control for 2 h prior to lysis for total RNA. Transcript levels were quantified by qPCR and normalized to HPRT as a reference gene. Data is represented as the fold change in target transcript expression relative to the untreated vector control and was quantified using the ΔΔCq method. An unpaired t-test was performed, ±SEM; n=3, *=P<0.05. C: HeLa Tet-Off cells were co-transfected with expression plasmids for an ARE-containing firefly luciferase plasmid (pTRE-Fluc-ARE) and a stable renilla luciferase plasmid (pTRE-Rluc). 36 h post transfection, doxycycline (Dox) was added to halt reporter gene transcription of both luciferase reporters, at the same time Torin (250 nM) or DMSO were added; 12 h after Dox addition, lysates were harvested in passive lysis buffer (Promega). Luciferase activity for both firefly and renilla was analyzed using the Dual-Luciferase Reporter Assay (Promega) and normalized (firefly/renilla) relative luciferase was calculated in relative light units (RLUs). Results were plotted using GraphPad, an unpaired t-test was performed, ±SEM; n=6, ***=P<0.001. D&E: HeLa Tet-Off cells were transduced with recombinant lentiviruses expressing either shRNAs targeting Atg5 or Atg14 (shAtg5, shAtg14) or a non-targeting control

(NS) and selected with puromycin (1 µg/mL). After selection, cells were co-transfected and Dox treatment was performed as described in C, except that co-transfection also included an expression plasmid for KapB or an empty vector control. Results were plotted using GraphPad, an unpaired t-test was performed, ±SEM; n=3, *=P<0.05, **=P<0.01. F: Cells were co-transfected as in E and bafilomycin (10 nM) was added at the same time as Dox. Results were plotted in GraphPad and a Student's t-test was performed, ±SEM; n=3, *=P<0.05, **=P<0.01.

Figure 4: Dcp1a protein levels are decreased by KapB expression and Torin treatment. A: HUVECs were treated with DMSO or Torin (250 nM) for 4 h prior to harvest. Samples were lysed in 2x Laemmli buffer and resolved by SDS-PAGE before immunoblotting with Xrn1, EDC4/Hedls, Dcp1a, and DDX6. Samples were quantified by normalizing the PB resident protein levels to the total protein in each lane and then the DMSO control using ImageLab (Biorad). Results were plotted in GraphPad and a one-way ANOVA was performed ±SEM; n=3, **=P<0.01. B: HUVECs were transduced with recombinant lentiviruses expressing either KapB or an empty vector control and selected with blasticidin (5 µg/mL). Cells were treated with DMSO or bafilomycin A1 (BafA1, 10 nM) for 4 h prior to harvest in 2x Laemmli buffer. Samples were resolved by SDS-PAGE and immunoblot was performed for Dcp1a or p62 (autophagy marker). Samples were quantified by normalizing Dcp1a protein levels to the total protein in each lane using Image Lab (Biorad) and then to the Vector DMSO control. Results were plotted in GraphPad and a 2-way ANOVA was performed, ±SEM; n=3, ***=P<0.001. C: HUVECs were transduced with recombinant lentiviruses expressing either KapB or an empty vector control and selected with blasticidin (5 µg/mL). Samples were harvested in 2x Laemmli buffer, resolved by SDS-PAGE and immunoblot was performed for Xrn1, Hedls/EDC4, or DDX6. Samples were quantified by normalizing Dcp1a protein levels to the total protein in each

lane using Image Lab (Biorad) and then to the Vector DMSO control. Results were plotted in GraphPad. D: HUVECs were sequentially transduced: first with recombinant lentiviruses expressing either shRNAs targeting Atg5 (shAtg5) or a non-targeting control (NS) and selected with puromycin (1 µg/mL), and second with either KapB or an empty vector control and selected with blasticidin (5 µg/mL). Samples were harvested in 2x Laemmli buffer and resolved by SDS-PAGE. Immunoblot was performed for Dcp1a, Atg5, and KapB. Samples were quantified by normalizing Dcp1a protein levels to the total protein in each lange using Image Lab (Biorad) and then to the Vector NS control. Results were plotted in GraphPad and a 2-way ANOVA was performed, ±SEM; n=3, *=P<0.05, **P=<0.01.

Figure 5. KapB-mediated PB disassembly and ARE-mRNA reporter expression require the selective autophagy receptor NDP52. A: HUVECs were sequentially transduced with recombinant lentivirus expressing KapB or an empty vector control and selected with blasticidin (5 µg/mL), and second with shRNAs targeting NDP52, OPTN, p62 or a non-targeting control (NS) and selected with puromycin (1 µg/mL). Coverslips were fixed in 4% paraformaldehyde, permeabilized in 0.1% Triton X-100 and immunostained for Hedls (PBs; white), DAPI (nuclei, blue). Scale bar=20 µm. Cells were imaged and the mean number of Hedls puncta per cell were quantified using CellProfiler. Data were plotted in GraphPad as the mean number of Hedls puncta per cell per condition ± SEM; n=3. A 2-way ANOVA was performed with a Šidák's multiple comparison test; * = P<0.05 **= P<0.01. B: HUVECs were transduced with recombinant lentivirus expressing an shRNA targeting NDP52 and selected with puromycin (1 µg/mL). Cells were treated with Torin (250 nM) or a DMSO control for 2 h prior to fixation in 4% paraformaldehyde and permeabilization in 0.1% Triton X-100. Samples were immunostained for Hedls (PBs; white), DAPI (nuclei, blue). Scale bar=20 µm. Cells were

946 imaged and the mean number of Hedls puncta per cell were quantified using CellProfiler. Data
947 were plotted in GraphPad as the mean number of Hedls puncta per cell per condition. Results
948 were plotted in GraphPad, a 2-way ANOVA was performed with a Šidák's multiple comparison
949 test, ± SEM; n=3. * = P<0.05. C: HeLa Tet-Off cells were transduced with recombinant
950 lentivirus expressing shRNAs targeting NDP52, OPTN, p62 or a NS control and selected with
951 puromycin (1μg/mL) then cells were co-transfected, treated with Dox and luciferase activity was
952 recorded and analyzed as in Figure 3. Data were plotted in GraphPad as the mean fold change in
953 the relative luciferase activity of each condition compared to vector NS or KapB NS; n=3. An
954 unpaired t-test was performed; * = P<0.05 **= P<0.01. D: Schematic of NDP52. NDP52
955 contains the following domains and interacting regions: SKICH domain (SKIP-carboxyl
956 homology domain), CLIR (non-canonical LC3-interaction motif), coiled-coil domain, GALB
957 (galectin binding domain) ZF1 & ZF2 (zinc finger domains). Known mutations that disrupt
958 NDP52 function include: V136S which prevents binding to LC3-C and C443K which prevents
959 binding to ubiquitin. E: HUVECs were sequentially transduced first with recombinant lentivirus
960 expressing shDNP52 targeting the 3'-UTR of NDP52 or a NS control and selected with
961 blasticidin (5 μg/mL), and second, with KapB and one of the following: mCherry control (mCh),
962 RFP-NDP52 wt, mCh-NDP52 C443K or mCh-NDP52 V136S/C443K. Coverslips were fixed
963 with 4% paraformaldehyde, permeabilized with 0.1% Triton X-100, and immunostained with
964 Hedls (PBs, green). Scale bar=20 μm. F: Samples from E were quantified; Hedls puncta were
965 counted using CellProfiler and normalized to the number of nuclei, results were plotted in
966 GraphPad, a 2-way ANOVA was performed with a Šidák's multiple comparison test, ± SEM;
967 n=3. * = P<0.05, **=P<0.01.

Figure 6: MK2EE-mediated PB disassembly does not require NDP52 or canonical autophagy. A: HUVECs were transduced with recombinant lentiviruses expressing either constitutively active MK2 (MK2EE) or an empty vector control and selected with blasticidin (5 µg/mL) for 48 h. Cells were treated with DMSO or bafilomycin A1 (10 nM) for 30 min before being fixed in methanol. Immunofluorescence was performed for LC3 (autophagosomes, white) and DAPI (nuclei, blue). Scale bar=20 µm. Total LC3 area per field was quantified by identifying LC3 puncta using CellProfiler and normalizing to the number of nuclei and the vector DMSO control. Results were plotted in GraphPad and a 2-way ANOVA was performed with a Šidák's multiple comparison test, ±SEM n=3; *=P<0.05. B: HUVECs were transduced with recombinant lentiviruses expressing either MK2EE or an empty vector control and selected with blasticidin (5 µg/mL). Cells were treated with bafilomycin A1 (10 nM) or a vehicle control (DMSO) for the indicated times prior to harvest in 2x Laemmli buffer. Protein lysates were resolved by SDS-PAGE and immunoblot was performed for p62 and LC3. Samples were quantified using Image Lab (Biorad) software and then normalized, first to total protein and then to their respective starting points (time 0 h). Results were plotted in GraphPad and a linear regression statistical test was performed, ±SEM; n=3, *=P<0.05, **=P<0.01. C: HUVECs were sequentially transduced: first with recombinant lentiviruses expressing either shRNAs targeting Atg5 (shAtg5) or a non-targeting control (NS) and selected with puromycin (1 µg/mL), and second, with either MK2EE or an empty vector control and selected with blasticidin (5 µg/mL). Coverslips were fixed in 4% paraformaldehyde, permeabilized in 0.1% Triton X-100, and immunostained for the PB-resident protein Hedls (PBs, white) and DAPI (nuclei, blue). Scale bar=20 µm. Hedls puncta were counted using CellProfiler and normalized to the number of nuclei, results were plotted in GraphPad and a 2-way ANOVA was performed with a Šidák's

multiple comparison test, ±SEM n=5; *=P<0.05. D: HeLa Tet-Off cells were transduced with recombinant lentiviruses expressing either shRNAs targeting Atg5 (shAtg5) or a non-targeting control (NS) and selected with puromycin (1 µg/mL) then co-transfected with expression plasmids for pTRE-Fluc-ARE, pTRE-Rluc, and MK2EE or an empty vector control, and treated as in Figure 3. Results were plotted using GraphPad, a Student's t-test was performed, ±SEM, n=4; *=P<0.05. E: HUVECs were sequentially transduced with recombinant lentivirus expressing shRNAs targeting NDP52, OPTN, p62 or a non-targeting control (NS) and selected with puromycin (1 µg/mL) and second with recombinant lentivirus expressing constitutively active MK2EE or an empty vector control and selected with blasticidin (5 µg/mL). Coverslips were fixed in 4% v/v paraformaldehyde, permeabilized in 0.1% Triton X-100, and immunostained for Hedls (PBs, white) and DAPI (nuclei, blue). Scale bar = 20 µm. Hedls puncta were counted using CellProfiler and normalized to the number of nuclei, results were plotted in GraphPad, ±SEM; n=3. F: HeLa Tet-Off cells were transduced with recombinant lentivirus expressing shRNAs targeting NDP52, OPTN, p62 or a NS control and selected with puromycin (1µg/mL) then cells were co-transfected, treated with Dox and luciferase activity was recorded and analyzed as in Figure 3. Data were plotted in GraphPad as the mean fold change in the relative luciferase activity of each condition compared to vector NS or MK2EE NS; n=3. An unpaired t-test was performed; * = P<0.05 **= P<0.01.

Figure 7: Model of NDP52-dependent PB disassembly elicited by KapB. A: KapB expression has the potential to impact two pathways that lead to PB disassembly, thereby increasing the stability/translation of AU-rich containing inflammatory cytokine mRNA. The first pathway is dependent on canonical autophagy and the SAR, NDP52, and is also used to elicit PB disassembly by the mTOR inhibitor, Torin. Because of its ability to bind and activate MK2,

KapB also may promote PB disassembly using an autophagy-independent pathway that relies on phosphorylated, active MK2, a pathway that is mimicked by overexpression of MK2EE. B: Under normal conditions, the cytoplasm of all cells contain PBs, granules comprised of RNA and RNA decay proteins that are visible by immunofluorescent microscopy. When KapB is expressed, microscopically visible PBs are lost but can reform after overexpression of Dcp1a-GFP or after stress-induced translation shutoff. PB disassembly elicited by KapB depends on the selective autophagy receptor, NDP52. KapB expression decreases the steady-state level of the PB protein, Dcp1a, but does not markedly alter the levels of other PB proteins like DDX6, ECD4/Hedls, or Xrn1. Dcp1a has been shown to be modified by phosphorylation and ubiquitination (Tenekeci *et al*, 2016; Aizer *et al*, 2013; Chiang *et al*, 2013) and these modifications alter PB formation and function. These data lead us to propose the following model. KapB expression leads to an as yet undetermined post-translational modification that promotes its recognition by the selective autophagy receptor, NDP52. Simultaneous binding of NDP52 to modified Dcp1a (or another unidentified PB protein) and to LC3 on the nascent phagophore recruit Dcp1a to the autophagosome for degradation. The loss of Dcp1a or another PB protein via selective autophagy leads to PB disassembly but does not prevent *de novo* PB assembly under stress, even during KapB expression.

DDX6/Rck: RNA helicase, EDC4/Hedls: decapping co-factor, Dcp2: catalytic component of decapping machinery, Dcp1a: decapping co-factor, ECD3: decapping enhancer, Xrn1: 3'-5' exonuclease.

Tables

Table 1: Drugs

Drug	Vendor/Catalogue #	Concentration
Torin1	Sigma-Aldrich 475991	250 nM
Bafilomycin A1	Sigma-Aldrich B1793	10 nM
Chloroquine	Sigma-Aldrich C6628	25 µM
MG-132	Selleckchem S2619	5 µM
LPS	Sigma-Aldrich L3129	1 µg/mL
Sodium Arsenite	Sigma-Aldrich 1.06277	0.25 mM
Doxycycline	Sigma-Aldrich D9891	1 µg/mL

Table 2: Plasmids

Plasmid	Use	Source	Mammalian Selection
pBMN mCh NDP52 C443K	UBD mutant	Addgene #119685 (Padman et al., 2019)	N/A
pBMN mCh NDP52 C443K V136S	UBD/LIR mutant	Addgene #119686 (Padman et al., 2019)	N/A
RFP-NDP52	Overexpression	Dr. Andreas Till (University Hospital of Bonn)	N/A
pcDNA 3.1 (+)	Empty Vector Control	Invitrogen V79020	N/A
pcDNA KapB BCBL1	ARE-mRNA stability	(Corcoran et al., 2015)	N/A
pcDNA FLAG-MK2EE	ARE-mRNA stability	(Corcoran et al., 2015)	N/A
pLKO.1-TRC	shRNA expression	Addgene #10878 (Moffat et al., 2006)	Puromycin
pLKO.1-blast	shRNA expression	Addgene #26655 (Bryant et al., 2010)	Blasticidin
pLJM1	Empty Vector Control	(Johnston et al., 2019)	Blasticidin/ Puromycin
pLJM1 KapB (pulmonary KS)	Overexpression	Cloned from pBMNIP-KapB (Corcoran et al., 2015) into pLJM1-BSD	Blasticidin

Plasmid	Use	Source	Mammalian Selection
pLJM1 mCh	Overexpression Control	Craig McCormick (Dalhousie University)	Blasticidin
pLJM1 FLAG-MK2EE	Overexpression	Cloned into pLJM1 using BamHI and EcoRI from pBMN FLAG-MK2EE (Corcoran et al., 2015)	Blasticidin/ Puromycin
pLJM1 RFP-NDP52	Overexpression	Cloned into pLJM1 using NheI and BamHI from RFP-NDP52	Puromycin
pLJM1 mCh-NDP52 C443K	Overexpression	Cloned into pLJM1 from Addgene #119685 using the primers listed in Table 4	Blasticidin/ Puromycin
pLJM1 mCh-NDP52 C443K V136S	Overexpression	Cloned into pLJM1 from Addgene #119686 using the primers listed in Table 4	Blasticidin/ Puromycin
pMD2.G	Lentivirus generation	Addgene #12259	N/A
psPAX2	Lentivirus generation	Addgene #12260	N/A
pTRE2 Firefly Luciferase-ARE	ARE-mRNA stability	(Corcoran et al., 2011)	N/A
pTRE2-Renilla Luciferase	ARE-mRNA stability	(Corcoran et al., 2011)	N/A

Table 3: shRNA target sequences

shRNA target	shRNA sequence 5'→3'	Region
Non-targeting (NS)	AGCACAAGCTGGAGTACAACTA	
Atg5	CTTTGATAATGAACAGTGAGA	CDS
NDP52(1)	GAGCTGCTTCAACTGAAAGAA	CDS
NDP52(2)	GACTTGCCTATGGAAACCCAT	CDS
NDP52(3)	CCCTTTGTGAACTAAGTTCAA	3'-UTR
NDP52(4)	CCTGACTTGATACTAAGTGAT	3'-UTR
Optineurin (1)	GCACGGCATTGTCTAAATATA	CDS
Optineurin (2)	GCCATGAAGCTAAATAATCAA	CDS
p62	CCGAATCTACATTAAAGAGAA	CDS
NBR1 (1)	GCCAGGAACCAAGTTTATCAA	CDS
NBR1 (2)	CCATCCTACAATATCTGTGAA	CDS
VCP (1)	ACCGTCCCAATCGGTTAATTG	CDS
VCP (2)	AGATCCGTCGAGATCACTTTG	CDS

Table 4: Cloning primers

Primer	Primer Sequence

NDP52 C443K & C443K/V136S BamHI-Forward	5' TAAGCAGGATCCGCCACCATGGTGAGCAAG 3'
NDP52 C443K & C443K/V136S EcoRI-Reverse	5' TAAGCAGAATTCCAGAGAGAGTGTTTGAACACGT 3'

Table 5: Antibodies

Antibody	Species	Vendor/Catalogue #	Application	Dilution
Hedls	Mouse	Santa Cruz sc-8418	Immunofluorescence Immunoblot	1:1000 1:1000
KapB	Rabbit	A generous gift from Don Ganem	Immunofluorescence	1:1000
NDP52	Rabbit	CST 60732	Immunoblot	1:1000
p62	Rabbit	CST 7695	Immunoblot	1:1000
Dcp1a	Mouse	CST 15365	Immunoblot	1:500
DDX6	Rabbit	Bethyl A300-461	Immunoblot	1:1000
MK2	Rabbit	CST 12155	Immunofluorescence	1:1000
LC3B	Rabbit	CST 2775	Immunofluorescence Immunoblot	1:200 1:1000
Atg5	Rabbit	CST 2630	Immunoblot	1:1000
Atg14	Rabbit	CST 96752	Immunoblot	1:1000
OPTN	Rabbit	Abcam ab23666	Immunoblot	1:1000
Xrn1	Rabbit	Abcam ab231197	Immunoblot	1:1000
VCP	Rabbit	CST 2649	Immunoblot	1:1000
NBR1	Rabbit	CST 9891	Immunoblot	1:1000

Table 6: qPCR primers

Primer	Primer Sequence
HPRT-1- Forward	5’ CTTTCCTTGGTCAGGCAGTATAA 3’
HPRT-2 - Reverse	5’ AGTCTGGCTTATATCCAACACTTC 3’
18S - Forward	5’ TTCGAACGTCTGCCCTATCAA 3’
18S - Reverse	5’ GATGTGGTAGCCGTTTCTCAGG 3’
IL-6 - Forward	5’ GAAGCTCTATCTCGCCTCCA 3’
IL-6 - Reverse	5’ TTTTCTGCCAGTGCCTCTTT 3’
CXCL8 - Forward	5’ AAATCTGGCAACCCTAGTCTG 3’
CXCL8 - Reverse	5’ GTGAGGTAAGATGGTGGCTAAT 3’
IL-1β - Forward	5’ CTCTCACCTCTCCTACTCACTT 3’
IL-1β - Reverse	5’ TCAGAATGTGGGAGCGAATG 3’
COX-2 - Forward	5’ CCCTTGGGTGTCAAAGGTAA 3’
COX-2 - Reverse	5’ GCCCTCGCTTATGATCTGTC 3’

1050

1051

1052

1053

Supplemental Figure Legends

Figure S1: KapB expression promotes PB disassembly but does not prevent PB assembly. HeLa cells expressing a doxycycline-inducible GFP-Dcp1a were used to determine whether KapB prevented granule assembly or promoted disassembly. A: HeLa cells were transfected with either KapB or an empty vector control prior to inducing expression of GFP-Dcp1a with doxycycline (1 µg/mL). Cells were fixed 12 h post-induction and immunostained for Hedls (PBs, red) and KapB (blue). Scale bar=20 µm. B: GFP-Dcp1a expression was induced with doxycycline (1 µg/mL) in HeLa cells prior to transfection with either KapB or an empty vector control. Cells were fixed 12 h post-transfection and immunostained for Hedls (PBs, red) and KapB (blue). Scale bar=20 µm. C: HUVECs were transduced with recombinant lentiviruses expressing either Kaposin B (KapB) or an empty vector control and selected with blasticidin (5 µg/mL). Cells were treated with sodium arsenite (0.25 mM) or a vehicle control for 30 min prior to fixation in 4% paraformaldehyde and permeabilization in 0.1% Triton X-100. Scale bar=20 µm.

Figure S2: Canonical autophagy knockdown prevents KapB-mediated PB disassembly. A&B: HUVECs were sequentially transduced: first with recombinant lentiviruses expressing either shRNAs targeting Atg5 or Atg14 (shAtg5, shAtg14) or a non-targeting control (NS) and selected with puromycin (1 µg/mL), and second with either KapB or an empty vector control and selected with blasticidin (5 µg/mL). Samples were lysed in 2x Laemmli and resolved by SDS-PAGE. Samples were immunoblotted for Atg5 (A) or Atg14 (B). For Atg5 (A) samples were quantified by normalizing Atg5 protein levels to the total protein in each lane using Image Lab (Biorad) and then to Vector NS. Results were plotted in GraphPad, a 2-way ANOVA was

performed, ±SEM; n=3, ***=P<0.001. C: Atg5 +/+ (WT) and -/- (KO) MEFs were transduced as in A and harvested in 2x Laemmli buffer before being resolved by SDS-PAGE. Samples were probed for LC3, a representative blot is shown. D: Atg5 +/+ and -/- MEFs were transduced with recombinant viruses expressing KapB or an empty vector control and selected with blasticidin (5 µg/mL). Samples were fixed in 4% paraformaldehyde and permeabilized in 0.1% Triton X-100. Immunofluorescence was performed for Hedls (PBs, white) and DAPI (nuclei, blue). Scale bar=20 µm. Hedls puncta were counted using CellProfiler and normalized to the number of nuclei, results were plotted in GraphPad and a 2-way ANOVA was performed with a Šidák's multiple comparison test, ±SEM; n=3, *=P<0.05, **=P<0.01.

Figure S3: Canonical autophagy shRNA silencing in HeLa cells. A&B: HeLas were transduced with recombinant lentiviruses expressing either shRNAs targeting Atg5 or Atg14 (shAtg5, shAtg14) or a non-targeting control (NS) and selected with puromycin (1 µg/mL) prior to transfection with KapB or an empty vector for luciferase assays. Samples were lysed in 2x Laemmli buffer and resolved by SDS-PAGE before immunoblotting with Atg5 (A) or Atg14 (B). Representative blots are shown.

Figure S4: Selective autophagy receptor knockdown in HUVECs reveals that OPTN and p62 are not required for KapB-mediated PB disassembly. A&B: HUVECs were transduced with shRNAs targeting VCP, NBR1, or a non-targeting control (NS) and selected with puromycin (1 µg/mL), then transduced with an empty vector control or KapB and selected with blasticidin (5 µg/mL). Samples were lysed in 2x Laemmli buffer, resolved by SDS-PAGE, and immunoblotted for NBR1 (A) and VCP (B). Representative blots are shown, successful VCP knockdown was lethal, while NBR1 knockdown was not successful. C: HUVECs were transduced with shRNAs targeting NDP52 or a non-targeting control (NS) and selected with

puromycin (1 µg/mL), then transduced with an empty vector control or KapB and selected with blasticidin (5 µg/mL). Samples were lysed in 2x Laemmli buffer, resolved by SDS-PAGE, and immunoblotted for NDP52. D&E: HUVECs were transduced with shRNAs targeting p62, OPTN, or a non-targeting control (NS) and selected with puromycin (1 µg/mL), then transduced with an empty vector control or KapB and selected with blasticidin (5 µg/mL). Samples were lysed in 2x Laemmli buffer and resolved by SDS-PAGE. Samples were immunoblotted for p62 (D) and OPTN (E), representative blots are shown. F: HUVECs were transduced as in D and E. Coverslips were fixed in 4% paraformaldehyde, permeabilized in 0.1% Triton X-100 and immunostained for Hedls (PBs; white), DAPI (nuclei, blue). Scale bar=20 µm. G: HUVECs were transduced with recombinant lentiviruses targeting NDP52 or a non-targeting control (NS) and selected with puromycin (1 µg/mL). Samples were lysed in 2x Laemmli buffer, resolved by SDS-PAGE, and immunoblotted for NDP52 to confirm knockdown for paired Torin immunofluorescence experiments.

Figure S5: shRNA silencing of selective autophagy receptors in HeLa cells. A, B&C: HeLas were transduced with shRNAs targeting NDP52, OPTN, p62, or a non-targeting control (NS) and selected with puromycin (1 µg/mL) prior to transfection with KapB or an empty vector for luciferase assays. Samples were lysed in 2x Laemmli buffer, resolved by SDS-PAGE, and immunoblotted for NDP52 (A), p62 (B), and OPTN (C). Representative blots are shown.

Figure S6: NDP52 shRNA silencing and rescue in control HUVECs. A: Representative western blot of HUVECs transduced with an shRNA targeting the 3'UTR of NDP52 or a non-

targeting control (NS) and selected with puromycin (1 µg/mL), then co-transduced with an empty vector control and mCherry (mCh) or KapB and mCh. Samples were lysed in 2x Laemmli, resolved by SDS-PAGE, and immunoblotted for NDP52. B: HUVECs were sequentially transduced first with recombinant lentivirus expressing shDNP52 targeting the 3'-UTR of NDP52 or a NS control and selected with blasticidin (5 µg/mL), and second, with vector and one of the following: mCherry control (mCh), RFP-NDP52 wt, mCh-NDP52 C443K or mCh-NDP52 V136S/C443K. Coverslips were fixed with 4% v/v paraformaldehyde, permeabilized with 0.1% Triton X-100, and were immunostained with Hedls (PBs, green). Scale bar=20 µm. C: Hedls puncta were counted using CellProfiler and normalized to the number of nuclei, results were plotted in GraphPad.

Figure S7: shRNA silencing of canonical and selective autophagy genes in MK2EE-expressing cells. A: HUVECs were transduced with shRNAs targeting Atg5 or a non-targeting control (NS) and selected with puromycin (1 µg/mL), then transduced with an empty vector control or KapB and selected with blasticidin (5 µg/mL). Samples were lysed in 2x Laemmli buffer, resolved by SDS-PAGE, and immunoblotted for Atg5. A representative blot is shown. B: HeLas were transduced with recombinant lentiviruses expressing either shRNAs targeting Atg5 or a non-targeting control (NS) and selected with puromycin (1 µg/mL) prior to transfection with MK2EE or an empty vector for luciferase assays. Samples were lysed in 2x Laemmli buffer and resolved by SDS-PAGE before immunoblotting for Atg5. A representative blot is shown. C, D&E: HUVECs were transduced with shRNAs targeting NDP52, p62, OPTN, or a non-targeting control (NS) and selected with puromycin (1 µg/mL), then transduced with an empty vector control or MK2EE and selected with blasticidin (5 µg/mL). Samples were lysed in 2x Laemmli buffer and resolved by SDS-PAGE. Samples were immunoblotted for NDP52 (C), p62 (D), and

1145 OPTN (E), representative blots are shown. F: HUVECs were transduced with shRNAs as in
1146 D&E. Coverslips were fixed, permeabilized, and immunostained for Hedls (PBs; white), DAPI
1147 (nuclei, blue). Scale bar=20 μm. G, H&I: HeLas were transduced with shRNAs targeting
1148 NDP52, OPTN, p62, or a non-targeting control (NS) and selected with puromycin (1 μg/mL),
1149 then transfected with an empty vector control or MK2EE for luciferase assays. Samples were
1150 lysed in 2x Laemmli buffer, resolved by SDS-PAGE, and immunoblotted for NDP52 (G), p62
1151 (H), and OPTN (I). Representative blots are shown.

1152

1153

Figure 1

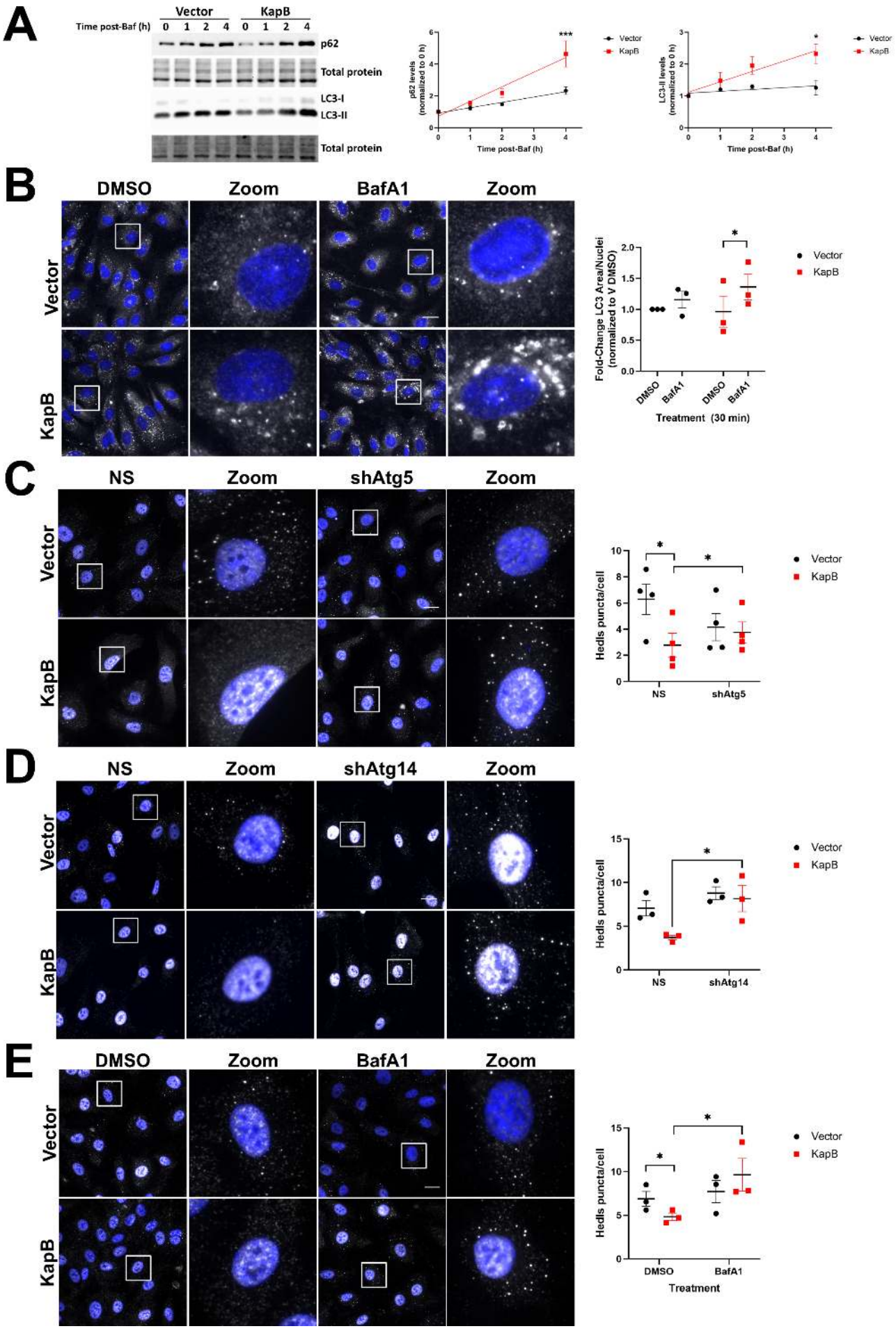

Figure 2

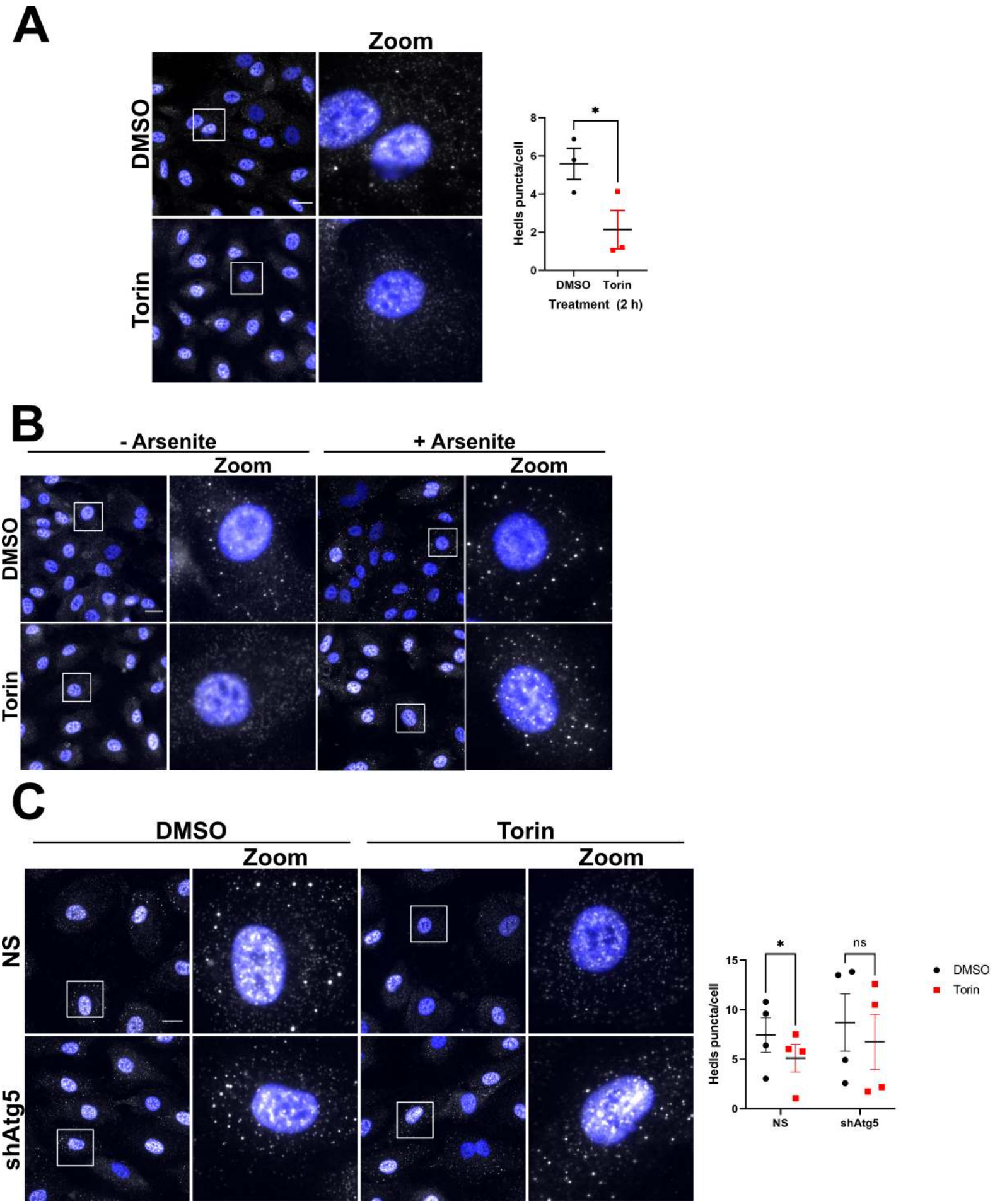

Figure 3

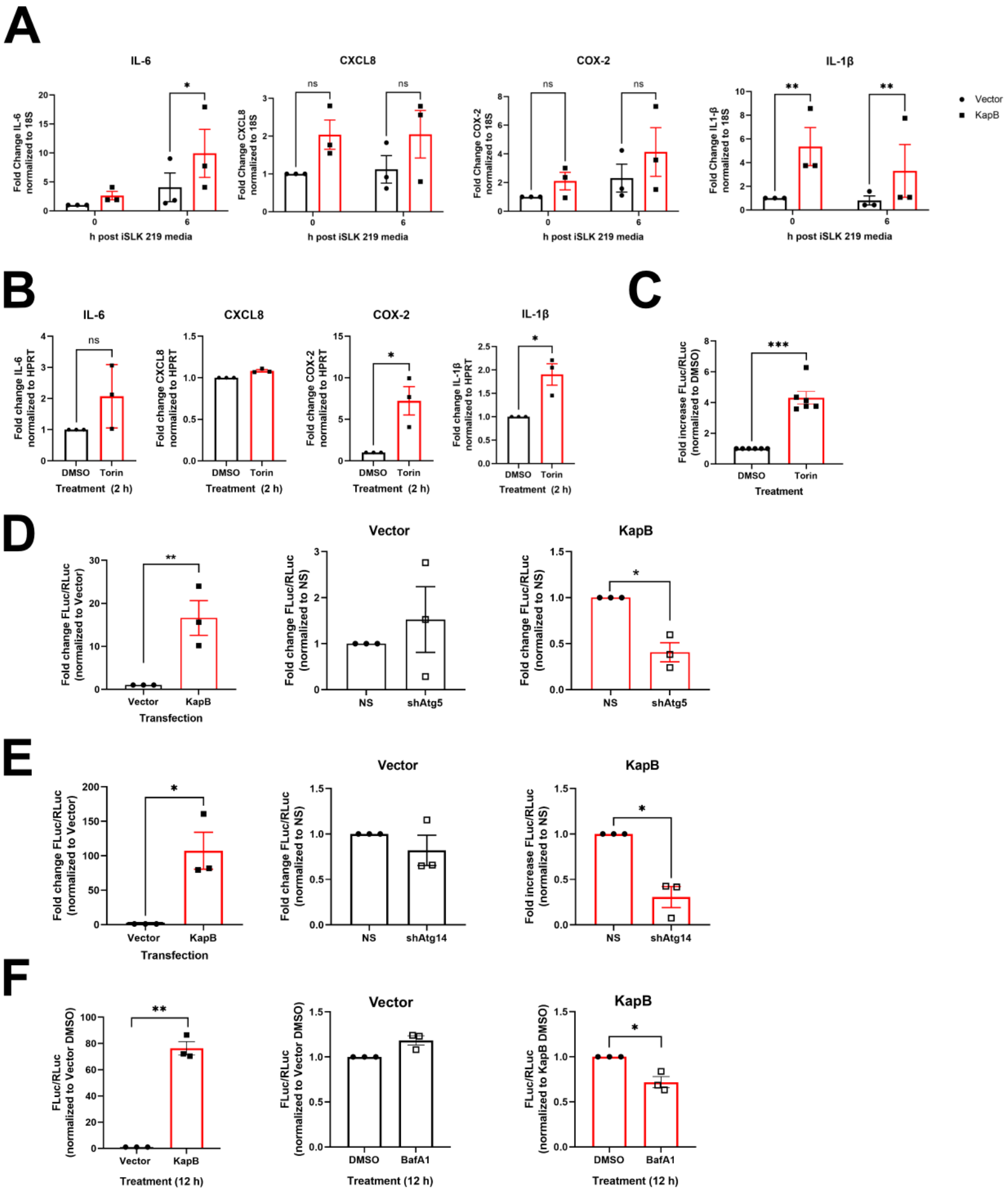

Figure 4

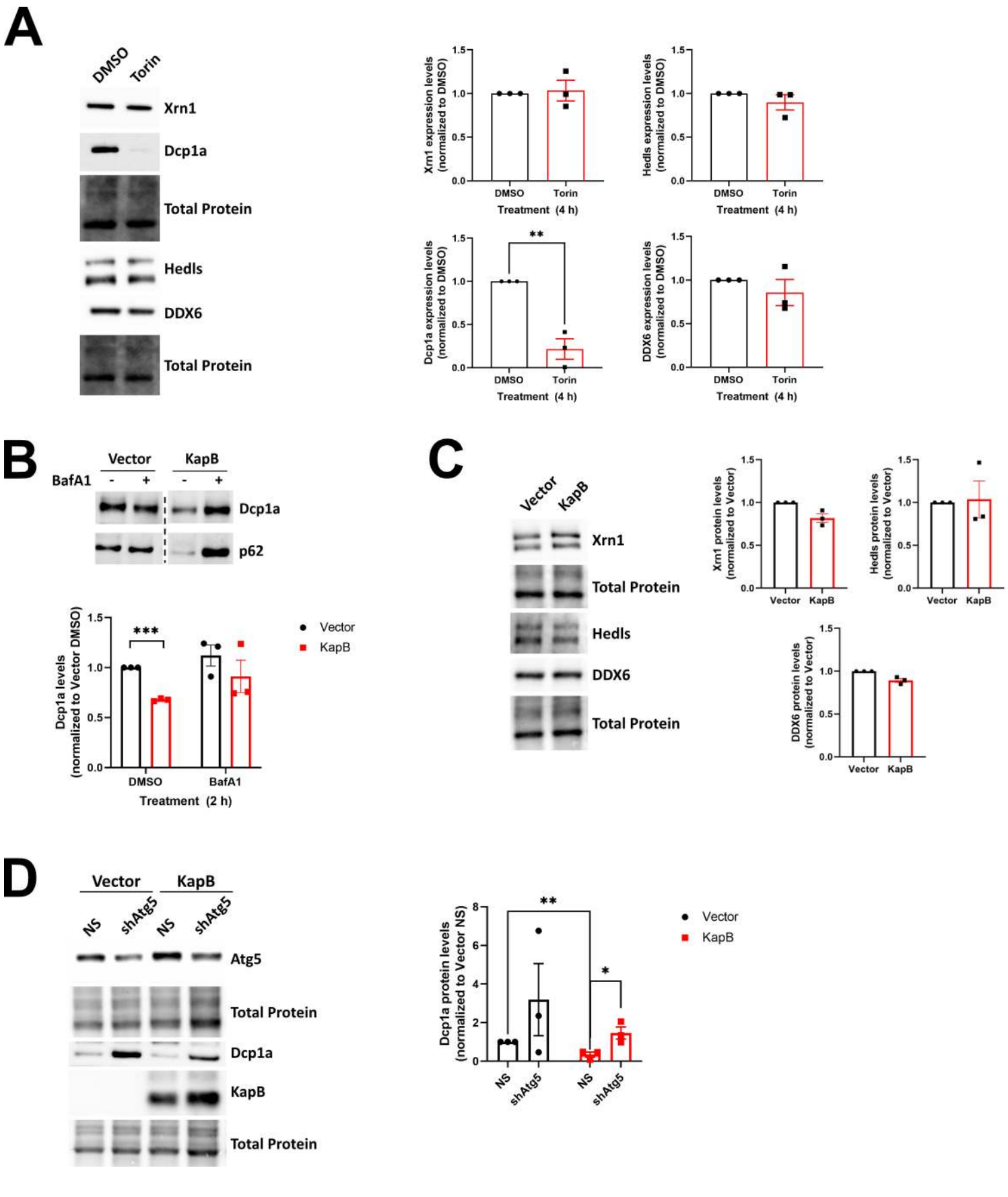

Figure 5

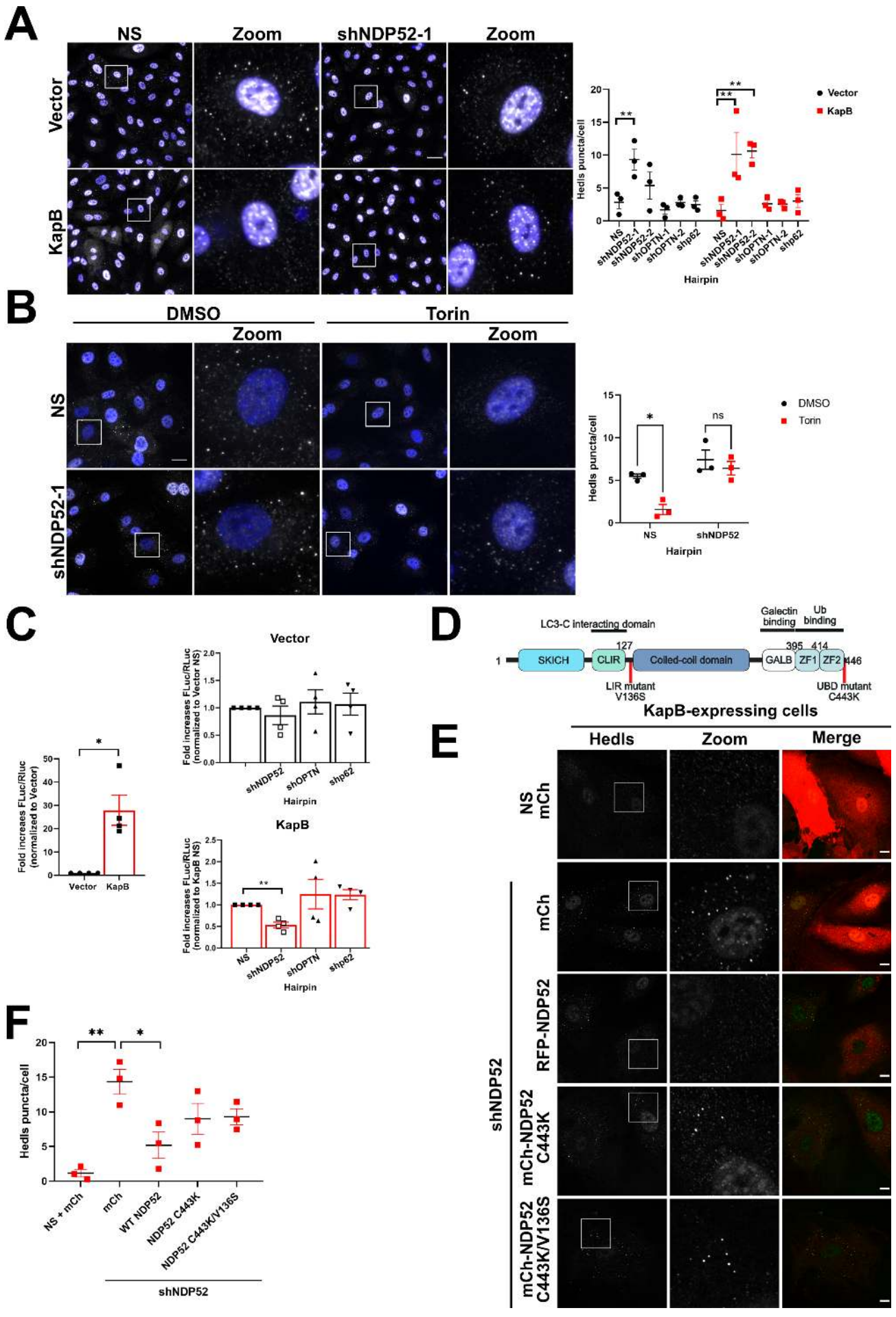

Figure 6

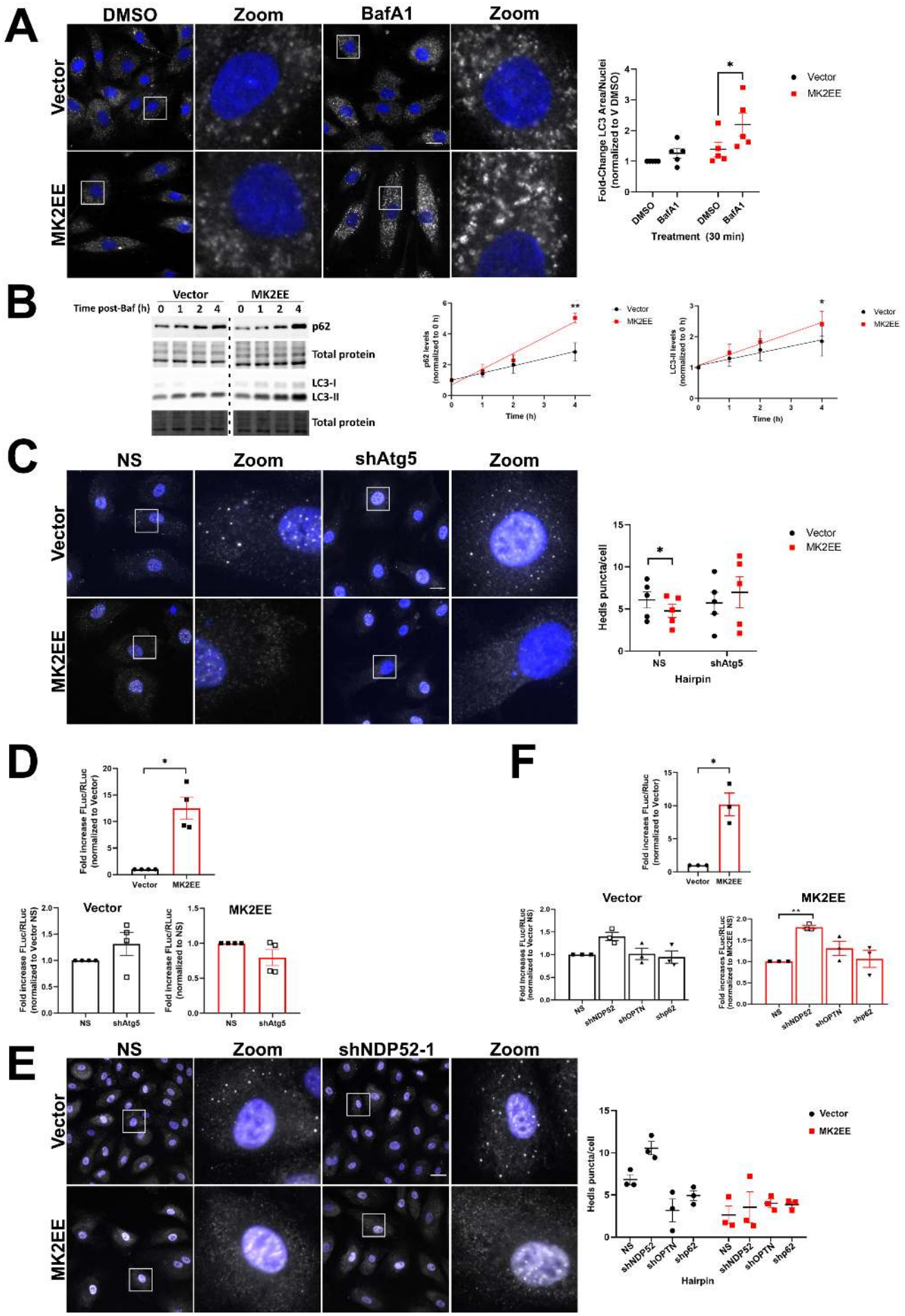

Figure 7

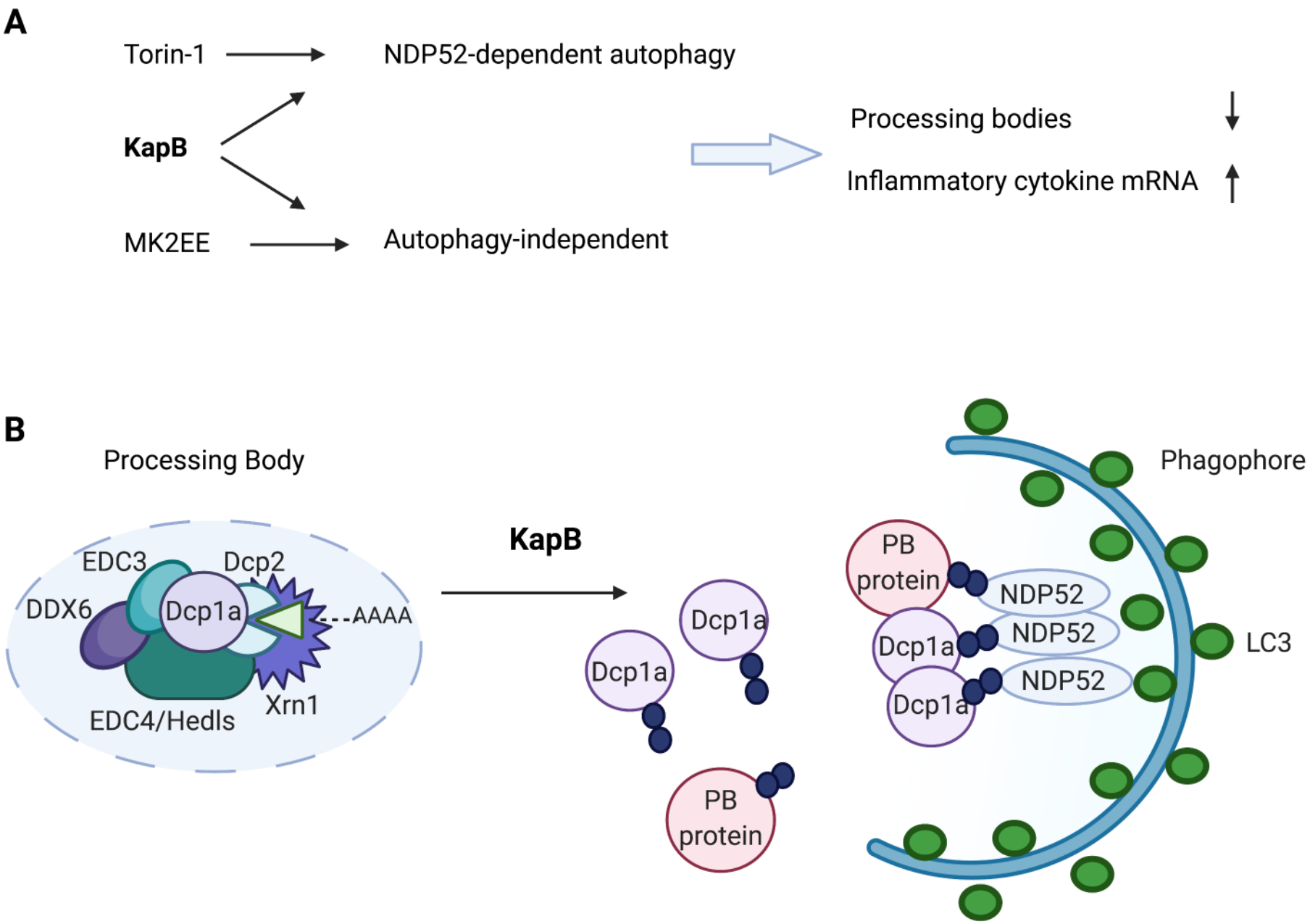
A
Torin-1
NDP52-dependent autophagy
KapB
MK2EE
Autophagy-independent
Processing bodies
Inflammatory cytokine mRNA
B
Processing Body
EDC3
Dcp2
DDX6
Dcp1a
AAAA
Xrn1
EDC4/Hedls
KapB
Dcp1a
Dcp1a
PB protein
Phagophore
PB protein
NDP52
Dcp1a
NDP52
Dcp1a
NDP52
LC3

Figure S1

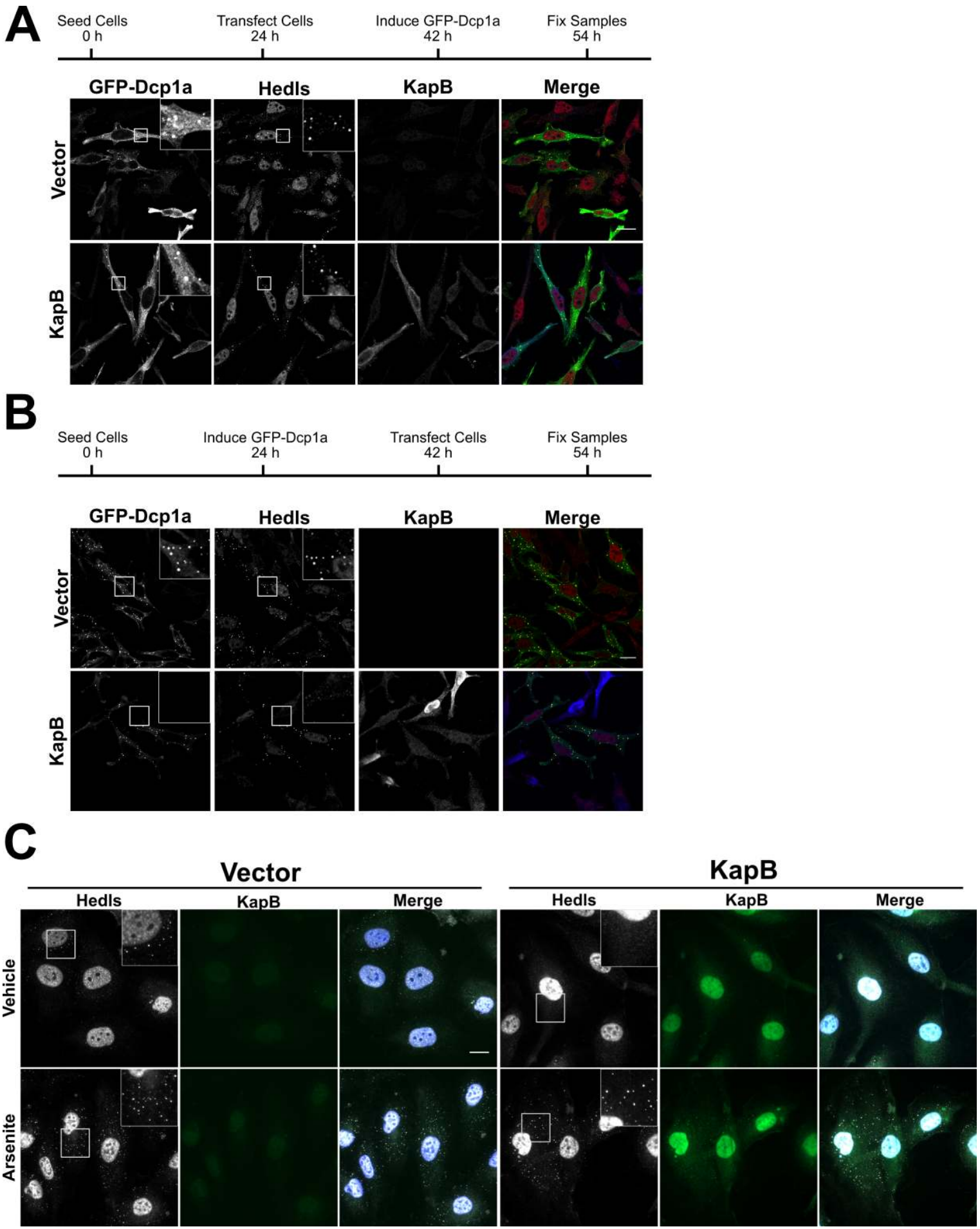

Figure S2

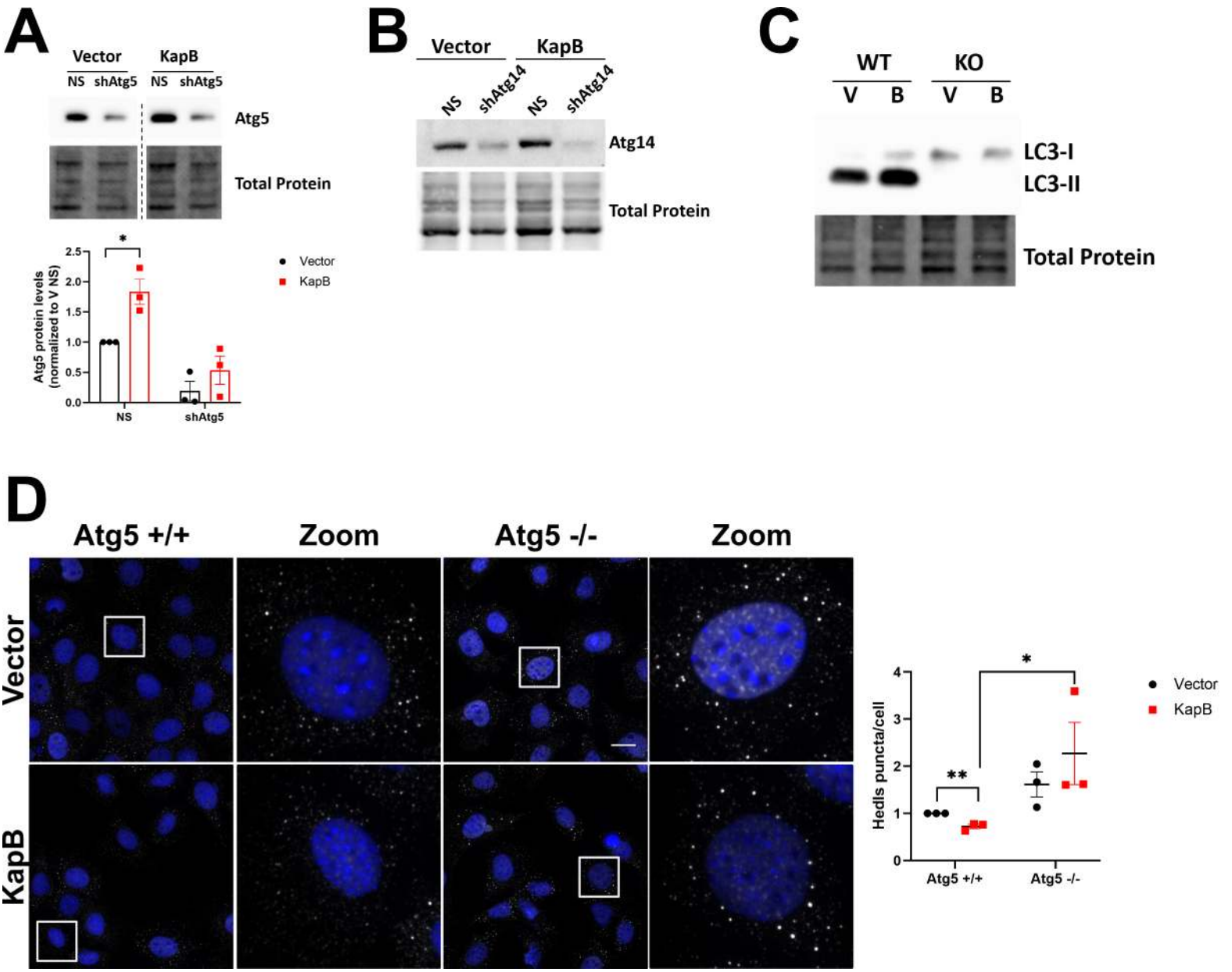

Figure S3

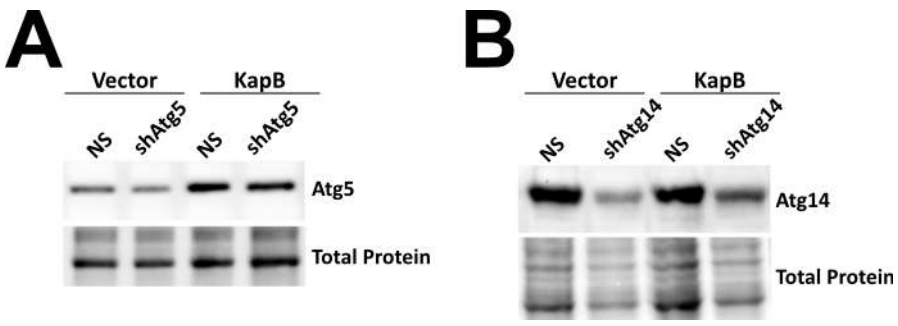

Figure S4

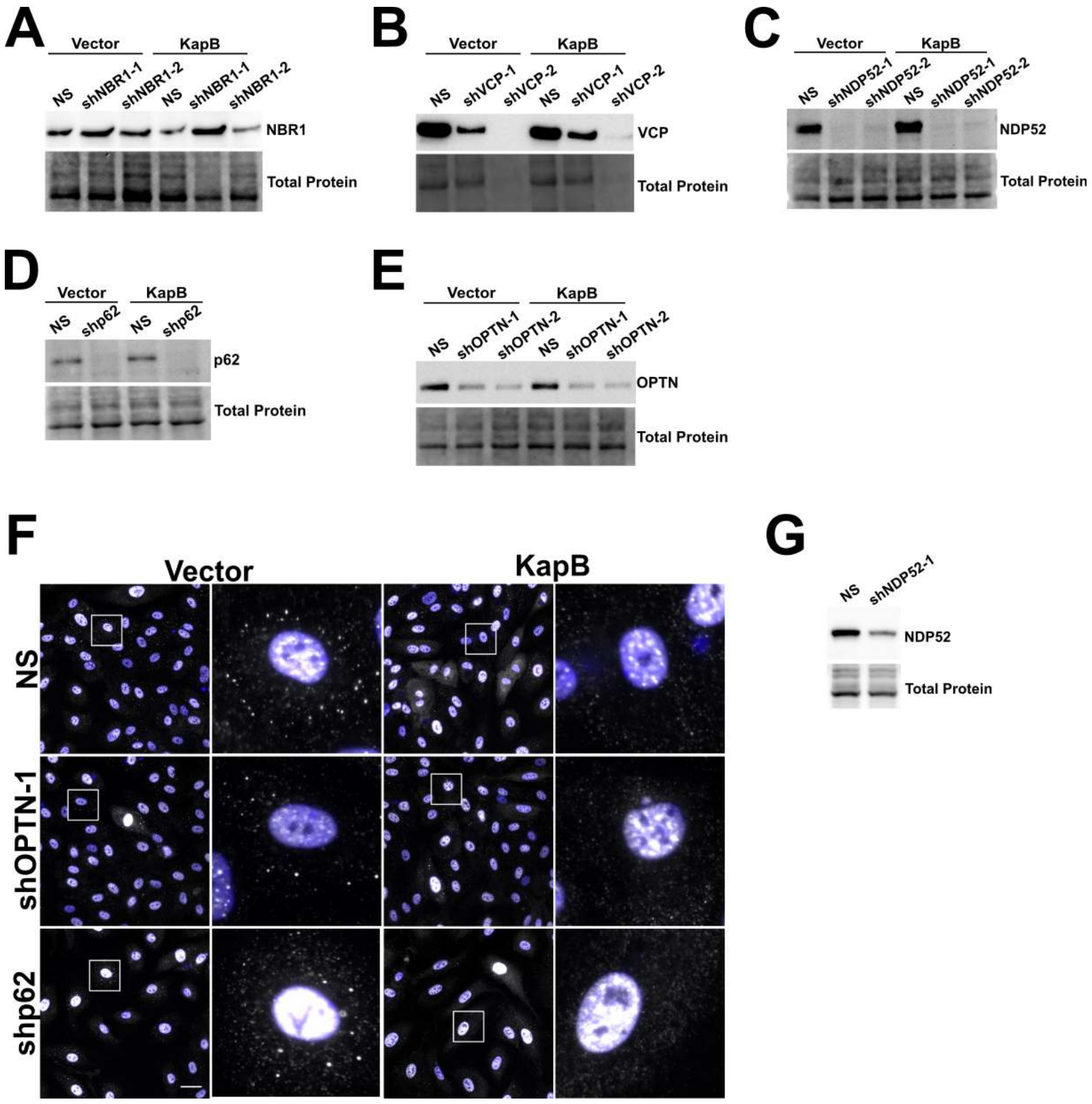

Figure S5

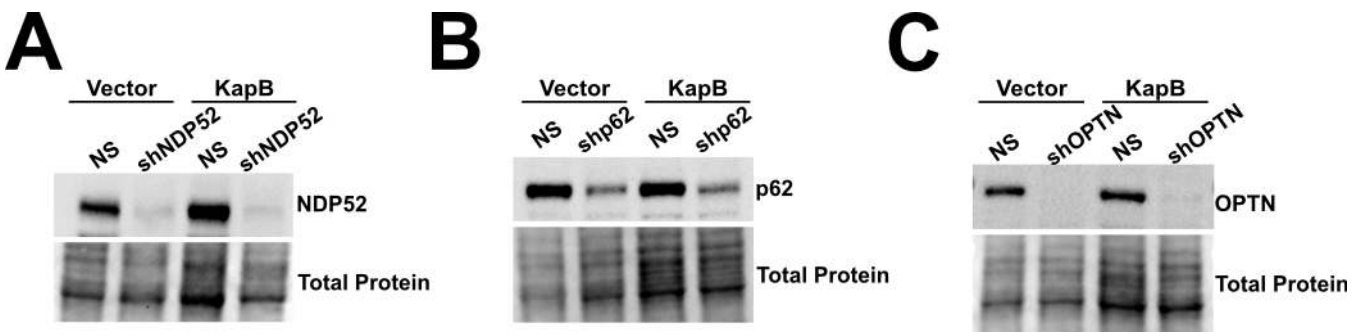

Figure S6

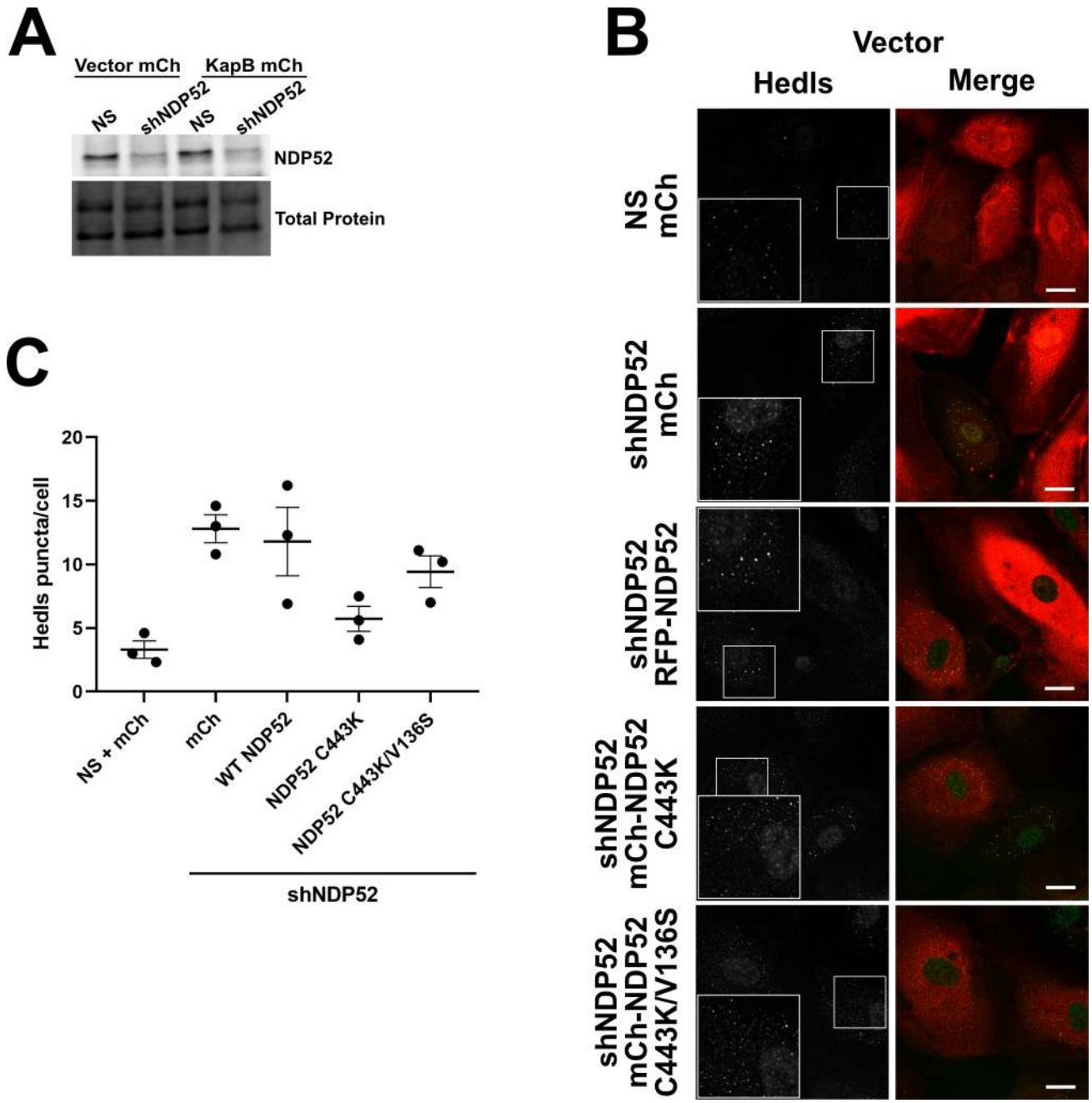

Figure S7